UNIVERSIDADE DE SÃO PAULO
INSTITUTO DE FÍSICA DE SÃO CARLOS

Pedro Luiz Mazo

Controlling the interaction via Feshbach resonances in a dual-species Bose-Einstein condensate: the implementation for potassium

São Carlos

2020

Pedro Luiz Mazo

Controlling the interaction via Feshbach resonances in a dual-species Bose-Einstein condensate: the implementation for potassium

Dissertation presented to the Graduate Program in Physics at the Instituto de Física de São Carlos, Universidade de São Paulo, to obtain the degree of Master in Science.

Concentration area: Basic Physics

Advisor: Prof. Dr. Kilvia Mayre Farias

Corrected Version

(original version available on the program Unit)

São Carlos

2020

Mazo, Pedro Luiz
Controlling the interaction via Feshbach resonances in a dual-species Bose-Einstein condensate: the implementation for potassium / Pedro Luiz Mazo; advisor Kilvia Mayre Farias - corrected version -- São Carlos 2020.
73 p.

Dissertation (Master's degree - Graduate Program in Basic Physics) -- Instituto de Física de São Carlos, Universidade de São Paulo - Brasil , 2020.

1. Feshbach resonances. 2. Bose-Einstein condensation. I. Farias, Kilvia Mayre, advisor. II. Title.

ACKNOWLEDGEMENTS

Este trabalho não seria possível sem a ajuda e apoio de meus amigos e família. Primeiro gostaria de agradecer aos meus pais Luiz Mazo e Marcia Mazo por me apoiarem durante todo o percurso, desde antes da graduação. Agradecer ao meu irmão João Mazo por sempre me incentivar e me apoiar durante minhas crises. Sou grato a minha irmã Raquel Mazo por sempre estar lá para conversar comigo durante os momentos difíceis. Também sou muito grato a minha vó Doracy Cordeiro que sempre me alegrava com seu sorriso e seu coração enorme.

Obrigado ao professor Vanderlei Bagnato por me receber na iniciação científica neste grupo cheio de pessoas brilhantes e estar sempre me motivando a ser cada vez melhor. Obrigado Kilvia Farias, por me ajudar desde a iniciação científica. Sempre esteve la para me ajudar e auxiliar nos momentos difíceis. Você me ajudou a ser um profissional melhor. Não consigo agradecer o suficiente. Obrigado Patrícia Castilho por sua amizade e toda a sua ajuda, paciência e compreensão durante todos estes anos. Paty você me ensinou muito. Sua disciplina e determinação sempre foram uma grande inspiração para mim. Obrigado Emmanuel Gutierrez, Emma! Sua amizade durante todo este tempo tornou o trabalho no laboratório divertido a ponto de eu não me importar de sair dela as nove da noite. Sou muito grato por tudo que você me ensinou, sei que será um grande cientista (mais do que já é hoje). Obrigado Edward Iraita, manito, sua amizade neste período de mestrado que percorremos juntos tornou tudo mais leve e divertido. Obrigado Gustavo de Oliveira, pela amizade e ajuda nas matérias onde batalhamos juntos. Obrigado por tudo, grupo NaK.

Também sou grato as pessoas que tiveram sua passagem no grupo. Edwin Penãfiel, Pedro Tavares, Humberto Duque, Vitor Monteiro, Franklin Vivanco, Pablo Dias, Guilherme Neto, todos vocês foram de grande ajuda e sou muito grato por isso e também pela amizade. Obrigado Johan, pela amizade e pelas alegres visitas ao lab. Obrigado ao grupo do BEC 1. Arnol García, sempre fazendo o melhor café do instituto. Obrigado por toda ajuda e pela amizade. Obrigado Michal Hemmerling por ser sempre uma pessoa gentil e divertida. Obrigado ao grupo do estrôncio, pela amizade e pelos cafézinhos compartilhados. Obrigado ao grupo do Liepo que me ensinaram muito sobre eletrônica e sempre tiveram muita paciência. Obrigado ao Leandro por sempre estar disposto a nos ajudar com um bom

humor.

Obrigado a todos os professores que tive durante a graduação e pós-graduação. Obrigado à equipe da pós graduação e da biblioteca pela ajuda e pelo excelente trabalho. Obrigado a todos os amigos que fiz na graduação, citar todos os nomes aqui seria loucura. Um obrigado especial ao time Fiscomp014, Galo, Ester, Fabio, Gabriel, Célia, Mino. Obrigado a todos que acabei esquecendo. Sou muito grato a todos.

Um agradecimento especial à CAPES pelo financiamento deste estudo. This study was financed in part by the Coordenação de Aperfeiçoamento de Pessoal de Nível Superior – Brasil (CAPES) – Finance Code 001.

A little knowledge is a dangerous thing;
drink deep, or taste not the pierian spring:
there shallow draughts intoxicate the brain,
and drinking largely sobers us again.
- Alexander Pope

ABSTRACT

MAZO, P. L. **Controlling the interaction via Feshbach resonances in a dual-species Bose-Einstein condensate:** the implementation for potassium. 2020. 73p. Dissertation (Master in Science) - Instituto de Física de São Carlos, Universidade de São Paulo, São Carlos, 2020.

In this work we document the first measure of Feshbach resonances in our laboratory utilizing potassium 39 in the state $F = 1, m_F = 0$. We submitted the 39K atoms trapped in an optical trap to a homogeneous magnetic field in the range of up to 800 Gauss, where are expected resonances for the species in the $|F = 1\rangle$ manifold. Those are the first steps to come up with a machine capable of using this technique for different and innovative studies on superfluidity in a mixture of quantum gases. In our case, we use the same pair of coils both to obtain different magnetic field gradients (phase of MOT and MT), in anti-Helmholtz configuration, as well as to obtain a homogeneous magnetic field (tuning the magnetic field around previewed resonance), in Helmholtz configuration. To make this possible, we have implemented a H-Bridge system, which consists in installing one of the coils in a system of power switches. We have prepared the atomic cloud since the MOT, passing through a Gray Molasses stage and reaching our Optical Dipole Trap with 10^6 atoms at 12 μK where we apply a homogeneous field and perform a loss spectroscopy. Here we will present the resonances we have obtained and its characterization.

Keywords: Bose-Einstein condensate. Feshbach resonance.

RESUMO

MAZO, P. L. **Controlando a interação em um condensado de Bose-Einstein de duas espécies através das ressonâncias de Feshbach:** a implementação para o potássio. 2020. 73p. Dissertação (Mestrado em Ciências) - Instituto de Física de São Carlos, Universidade de São Paulo, São Carlos, 2020.

Nesse trabalho documentamos as primeiras medidas das ressonâncias de Feshbach em nosso laboratório utilizando o potássio 39 no estado $F = 1, m_F = 0$. Nós submetemos os átomos de 39K aprisionados em uma armadilha óptica a um campo magnético homogêneo com um alcance de 800 G, onde é esperado que estejam as ressonâncias de Feshbach para a espécie atômica nos estados com $|F = 1\rangle$. Estes são os primeiros passos para compormos uma máquina capaz de usar esta técnica para diferentes e inovativos estudos em superfluidez em uma mistura de gases quânticos. Em nosso caso, nós usamos o mesmo par de bobinas para tanto obter diferentes gradientes (estágios de MOT e MT) em anti-Helmholtz, tanto para gerar um campo homogenêo em configuração Helmholtz (sintonizando o campo magnético nas ressonâncias ditas). Para tornar isto possível, nós implementamos uma ponte-H, que consiste na instalação de um sistema de interruptores de energia em uma das bobinas do par. Nós preparamos a nuvem atômica desde o MOT, passando pelo estágio da Gray Molasses e chegando na armadilha dipolar óptica com 10^6 átomos na temperatura de 12 μK onde aplicamos o campo homogêneo e performamos a espectroscopia de perda. Aqui nós apresentaramos as ressonâncias que medimos e a caracterização feita.

Palavras-chave: Condensado de Bose-Einstein. Ressonâncias de Feshbach.

LIST OF FIGURES

LIST OF ABBREVIATIONS AND ACRONYMS

AOM	Acoustic-Optical Modulator
BEC	Bose-Einstein Condensate
CMOT	Compressed Magneto-Optical Trap
FR	Feshbach Resonances
GM	Gray Molasses
IGBT	Insulated Gate Bipolar Transistor
MOPA	Master Oscillator Power Amplifier
MOT	Magneto-Optical Trap
MT	Magnetic Trap
ODT	Optical Dipole Trap
PID	Proportional–Integral–Derivative
PSD	Phase-space Density
SC	Science Chamber
SL	Scattering Length
VCO	Voltage-Controlled Oscillator

CONTENTS

1 INTRODUCTION

Since the first obtaining of a Bose-Einstein Condensate (BEC) in 1995,[1] ultracold atoms systems have received considerable attention among physicists. This type of system shows a enormous potential with a high degree of control, and ultra-low temperatures provide an ideal system for studying quantum phenomena. The quantum aspects of the matter are finally exposed in a macroscopic scale in the BEC, where there are still so much to be learned. Double species experiments add a new degree of both difficulty and possibility where the interaction between the species makes the problem more complex and interesting.[2–4] The discovery of Feshbach resonances[5,6] and how it can manipulate all the system's interactions simply by changing the magnetic field opened a new horizon of possibilities where all types of behaviours finally can be studied and (hopefully) understood.

In our laboratory, in the Center of Optics and Photonics in IFSC, we have developed various experiments towards Bose-Einstein Condensation of sodium[7–9] and rubidium[10–13] for many years. We have explored different aspects of collective excitations, thermodynamics in a trapped sample, vortex formation, and the achievement of quantum turbulence in ultracold gases. Looking at the advancing of these studies and going beyond, we invested in a system capable of obtaining a double condensate of sodium and potassium in recent years. This system intends to explore aspects such as phase separation, miscibility effects, and exploration of equilibrium systems, vortex formation, and quantum turbulence.

The main focus of this work is the tool capable of changing the interactions by a simple knob, the Feshbach resonances, where we document the implementation of the technique with the results obtained with the basic theory necessary to understand the physics behind it. Going from scattering theory to the different ways of tuning the resonances and finally showing the experimental results of the implementation of the technique. Although the experiment involves two species, this work will focus only on potassium, where we centralize the Feshbach tests. We will insert sodium in the near future. In the meanwhile, only one species is enough to guarantee the functionality of the technique.

In the second Chapter, we present a review of the collision and scattering theory. We go from the classical atom colliding with the quantum system of particles, giving

special attention to the scattering length, which will have great importance later. Then, we go to the Chapter 3 - The Feshbach resonances, where we give a brief introduction on the subject, first observed in nuclear physics, and then explain the famous two channel model. A simple "toy model" is used to give a better intuition about the phenomenon, presenting a few ways to detect a Feshbach resonance experimentally. Furthermore, we show the resonances listed for potassium 39 and how we plan to detect them. A brief explanation of the miscible and immiscible phenomenon is given to motivate the future work on a double species BEC.

In the Chapter 4 we present the laser setup used, with all the transitions and set-ups necessary in the laboratory. The instrumentals used in the tuning of the resonances is explained in detail. In Chapter 5 we show the results, going through all the steps from the beginning of the sequence to the Optical-Dipole Trap (ODT), where the resonances were tuned. We do a loss spectroscopy measurement and compare the effects of the change in the interaction by measuring lifetime of the atoms on the ODT in different situations. In conclusion, we compact the results and talk about the current state of the experiment and the prospects.

2 SCATTERING THEORY

Before we start on the theory behind the Feshbach resonances, a solid understanding of atomic collisions and scattering theory is necessary. In this Chapter, the reader will be reviewing some basic concepts that will be of great importance later. We start with the classical theory of collisions, and we transition to the quantum realm, talking about the scattering properties; the Hamiltonian utilized to the famous Lippmann-Schwinger equation. Finally, we go to low temperatures, focusing on the cross-section and scattering length. These two terms will be essential throughout the whole dissertation.

2.1 **A colliding system:** the channels of a collision

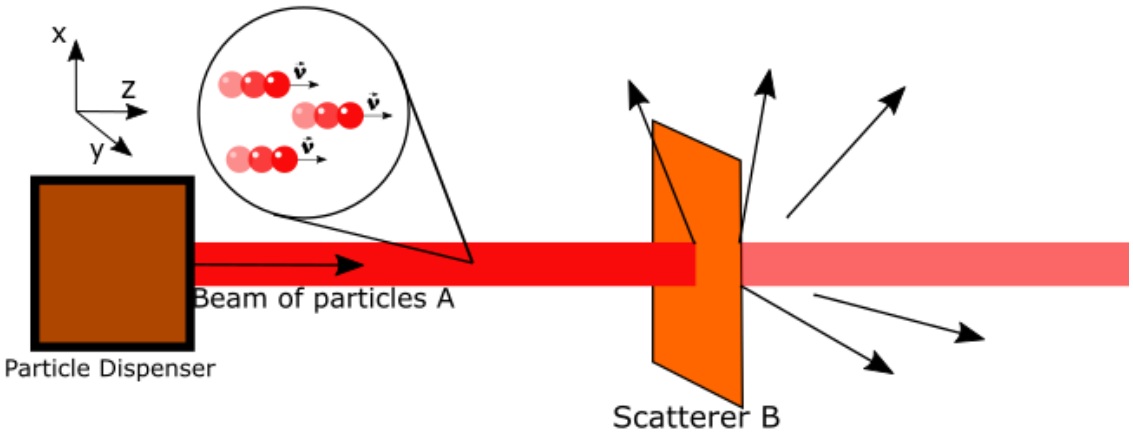

Figure 1 – The scattering process. A beam of collimated particles coming through a dispenser is colliding with a barrier. A fraction of the particles is scattered and the rest remains in the beam.

Source: By the author

The collision process can be described with two elements: the incident particle (or particles) and the scatterer (figure 1). When considering one type of incident particle and one scatterer, the collision process can be written in the following way:

$$A + B \rightarrow C + D$$

Let us say A is the incident beam of particles, and B is the scatterer. The different

configurations of $A+B$ constitutes the entrance channel, and the states of $C+D$ constitutes the exit channel. $C + D$ can be many things; in an elastic collision, $C + D$ would be the same as $A + B$ that started the collision, with the scatterer not interfering with the incident particle's energy or state. Similarly, the final state can have only one element C if the particle and scatterer were fused during the collision. The incident particle can also explode into six pieces by the scatterer; the final state would be $C+D+E+F+G+H+J$ counting the scatterer.

To characterize the collision, we can talk about the channels of the collision. A channel is the possible mode of fragmentation of the system during the collision.[14] Since the definition of the channels can involve some arbitrariness; one must be careful. Different states can be amounted into one channel or treated separately depending on the aspect of interest. One can treat the different excited states as different channels when treating with collisions, for example. In an elastic collision, the system remains in the initial channel. When a particular channel is energetically accessible, we call it an open channel, while the channels forbidden by energy conservation will be called a closed channel. This will be important when discussing the two-channels model for Feshbach resonance in the next chapter.

2.2 The cross section of a collision

One concept of great importance in our studies is the variable known as the collision cross section. The cross-section can be defined by the ratio of the number of certain events in a collision per unit time and per unit scatterer. To illustrate this concept, we shall look closely at a simple collision case where we have a beam of particles A with a sufficient number of particles with nearly parallel directions with the velocity peaked around a specific value v_i. If we call the cross section of the beam S and the number of particles A per unit volume n_a, we can write the flux of particles as:

$$\Phi_a = n_a v_i = \frac{N_a}{S} \tag{2.1}$$

Where N_a is the number of particles reaching the target per unit time. If we assume a target with thickness, l, sufficient small (a barrier of the scatterer particle B) and call n_b

the density of the particles in the barrier, we can write accordingly:

$$\mathcal{N}_b = S \cdot l \cdot n_b = S \cdot n'_b \tag{2.2}$$

The quantity $\mathcal{N}_b$ is the average number of particles B in the region of the beam of particles A, n'_b is the particles B's surface density. Under these conditions, we can see intuitively that the total number of particles A N_{tot} interacting with the scatterer is proportional to the flux of particles A and the total number of scatterers B. We may write:

$$N_{tot} = \Phi_a \cdot \mathcal{N}_b \cdot \sigma_{tot} \tag{2.3}$$

Where σ_{tot} is called the total cross section of the collision and has the dimension of an area, this quantity can be thought of as the "effective area" where the interaction can occur within the beam. However, one should not infer that it is directly correlated with the particles geometrical properties. Defining $P_{tot} = N_{tot}/N_a$ as the probability that an incident particle will interact with the scatterer, from equations 2.1 2.2 2.3):

$$P_{tot} = n'_b \cdot \sigma_{tot} \tag{2.4}$$

How the collision interactions will take place (or if it will interact at all) will be dictated by the total cross section, which will depend on intrinsic properties of the system A+B and the energy of the particles that will or will not be scattered. A more profound discussion will occur later, but now it would be useful to have the cross section as a differential. We will consider the laboratory flame of reference (illustrated in figure 1) and elastic collisions only.

$$dN = \Phi_a \cdot n_b \cdot \sigma(\theta, \phi) d\Omega \tag{2.5}$$

Where we write the differential cross section:

$$\sigma = \frac{d\sigma}{d\Omega} \tag{2.6}$$

The elastic cross section is obtained by integrating the differential elastic cross section over all scattering angles:

$$\sigma_{tot} = \int \frac{d\sigma(\theta,\phi)}{d\Omega} d\Omega = \int_0^{2\pi} \int_0^{\pi} \frac{d\sigma(\theta,\phi)}{d\Omega} sin(\theta) d\phi d\theta \tag{2.7}$$

2.3 The interatomic potential

Considering our case of interest that is the collision of cold neutral atoms, the interaction between them will be an induced dipole-dipole interaction, with a Van Der Waals type of potential: Attractive at long distances and very repulsive at short distances (see figure 2). For large distances, the interaction will become more and more negligible. After a certain point (called the Van Der Waals length[15]) the wavefunction is unaffected by the potential with good approximation.

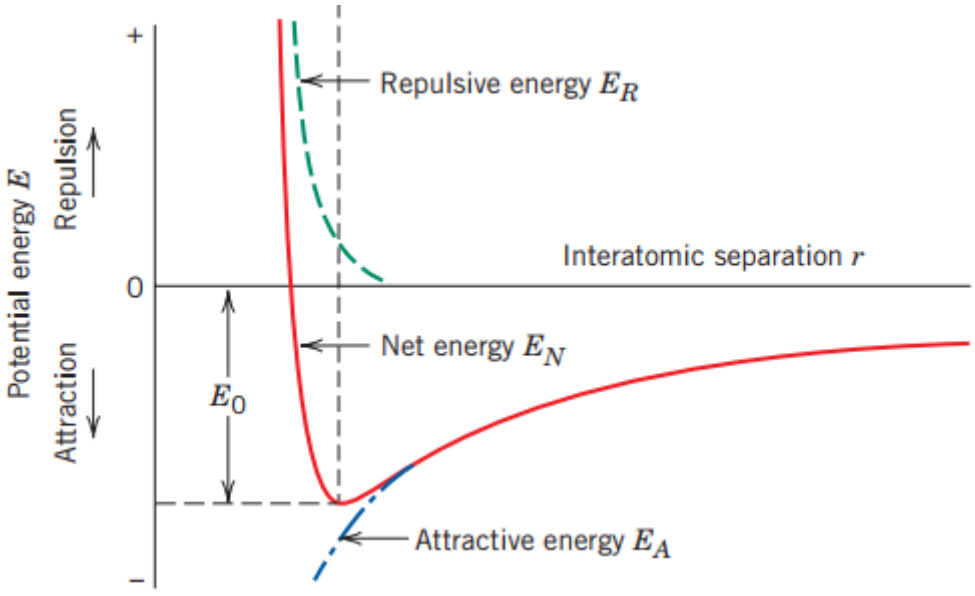

Figure 2 – The Van der Waals potential.
Source: Adapted from CALLISTER.[16]

The exact format of the potential is subject to the atoms' internal states in question, and different internal states can have multiple molecular potentials associated. These molecular potentials are closed channels; they support at least one bound state and are energetically inaccessible by the atoms during a collision.

2.4 A two-body problem

Now we shall look more directly into a collision of two particles, treating the non-relativistic collision and scattering through a potential $V(\mathbf{r})$. The potential depends on the relative motion of the two particles colliding. We will do the first to separate the problem into two parts: one corresponding to the relative motion between particles and one corresponding to the center of mass in the laboratory reference frame. We will assume the system to have reached a stationary state and relate the cross section to the asymptotic behaviour of the standing wave function.

Considering particle A with corresponding position and mass $\vec{r}_a$ and m_a and do the same for particle B ($\vec{r}_b$ and m_b) and considering the potential between then to be depending only on the relative position between particles ($\vec{r}_a - \vec{r}_b$) we can write the full Hamiltonian of the system:

$$\left(-\frac{\hbar^2\nabla^2_{r_a}}{2m_a} - \frac{\hbar^2\nabla^2_{r_b}}{2m_b} + V(\vec{r}_a - \vec{r}_b)\right)\Psi(\vec{r}_a, \vec{r}_b) = E\Psi(\vec{r}_a, \vec{r}_b) \tag{2.8}$$

Where E is the total energy of the system and $\Psi(\vec{r}_a, \vec{r}_b)$ the stationary wave function, $\hbar$ is the planck constant divided by 2π, μ is the reduced mass of the two particles, ϕ is the wave function, $V(r)$ is the potential energy between both particles and ∇^2_r is the Laplace operator. By changing variables ($(m_a\vec{r}_a + m_b\vec{r}_b)/(m_a + m_b) = \vec{R}$, $\mu = m_a m_b/(m_a + m_b)$, $\vec{r} = \vec{r}_a - \vec{r}_b$ and $M = m_a + m_b$) we can write the Hamiltonian as:

$$\left(-\frac{\hbar^2\nabla^2_R}{2M} - \frac{\hbar^2\nabla^2_r}{2\mu} + V(\vec{r})\right)\Psi(\vec{r}, \vec{R}) = E\Psi(\vec{r}, \vec{R}) \tag{2.9}$$

Then we can perform a separation of the wave function $\Psi(\vec{r}, \vec{R}) = \phi(r) \cdot \psi(R)$ since the Hamiltonian have a complete set of solutions in this form and the potential depends only on $\vec{r}$. Now we separate the Hamiltonian into two time-independent Schrödinger's equations:

$$\frac{-\hbar^2\nabla^2_R}{2M}\psi(\vec{R}) = E_{CM}\psi(\vec{R}) \tag{2.10}$$

and

$$\left(-\frac{\hbar^2\nabla^2_r}{2\mu} + V(\vec{r})\right)\phi(\vec{r}) = E_{rel}\phi(\vec{r}) \tag{2.11}$$

with $E = E_{CM} + E_{rel}$. We have successfully transformed a two-body problem into two

one-body problem. Equation 2.10 is the Hamiltonian of a free particle with the coordinates $\vec{R}$ and mass M while the equation 2.11 is the Hamiltonian of a wave function $\phi(\vec{r})$ with mass μ in the presence of a potential $V(\vec{r})$. Now the problem of scattering is reduced to the interaction of a particle with reduced mass μ and relative position $\vec{r}$ by a potential $V(\vec{r})$.

2.5 The Lippmann-Schwinger equation

Now that we have separated the problem into two one-body problem we can focus on solving equation 2.11 that is typically the Schrödinger equation for a particle in the presence of a potential $V(r)$. One relevant assumption being made here (that will be shown later to be correct) is that the collision is indeed elastic. The initial assumption implies that the solution of the Schrödinger equation shown above has the same eigenvalue of the energy of a free particle:

$$\begin{aligned} H\Psi(\vec{r}) &= \left(-\frac{\hbar^2\nabla_r^2}{2\mu} + V(\vec{r})\right)\Psi(\vec{r}) = E\Psi(\vec{r}) \\ H_{\text{Free}}\Phi(\vec{r}) &= -\frac{\hbar^2\nabla_r^2}{2\mu}\Phi(\vec{r}) = E\Phi(\vec{r}) \end{aligned} \tag{2.12}$$

We are looking for a solution that when $V \to 0 \Rightarrow \Psi(\vec{r}) \to \Phi(\vec{r})$ since we have a continuous energy spectra.[17] It can be verified (apply $E - H_{\text{Free}}$ to both sides) that the solution is:

$$|\Psi\rangle = \frac{1}{E - H_{\text{Free}}}V|\Psi\rangle + |\Phi\rangle \tag{2.13}$$

Since E is an eigenvalue of H_{Free} we make the denominator "a little complex" to avoid any possible divergence:

$$|\Psi\rangle = \frac{1}{E - H_{\text{Free}} \pm i\epsilon}V|\Psi\rangle + |\Phi\rangle \tag{2.14}$$

Finally 2.14 is the famous Lippman-Schwinger equation. Choosing a representation and solving this approximating for a large r we have the following solution[17]:

$$\begin{aligned} \langle \mathbf{x}|\mathbf{\Psi}\rangle &= \frac{e^{i\mathbf{k}\cdot\mathbf{x}}}{(2\pi)^{2/3}} - \frac{e^{ikr}}{r}\frac{2m}{4\pi\hbar^2}\int d^3x' e^{-i\mathbf{k'}\cdot\mathbf{x'}}V(\mathbf{x'})\langle \mathbf{x'}|\Psi\rangle \\ &= \frac{1}{(2\pi)^{2/3}}\left[e^{i\mathbf{k}\cdot\mathbf{x}} + \frac{e^{ikr}}{r}f(\mathbf{k'},\mathbf{k})\right] \end{aligned} \tag{2.15}$$

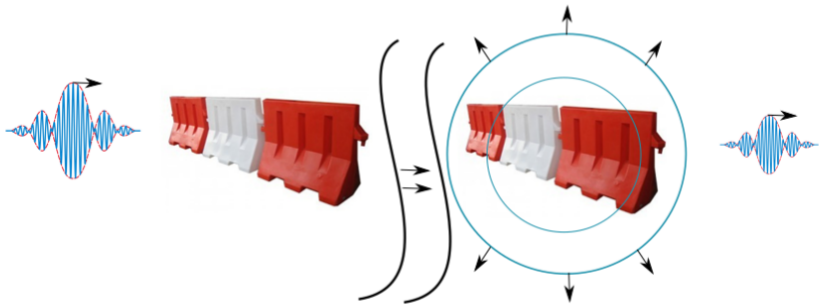

Figure 3 – Wave dynamics according to the equation 2.15 where we have a wave propagating towards a barrier and after the collision the wave is divided into two parts: One that continues propagating to the right and one spherical wave propagating outwards the barrier.

Source: By the author.

Where $f(\mathbf{k'},\mathbf{k})$ is the amplitude of the part of the wave that was scattered by the barrier going outwards as a spherical wave (see figure 3). The amplitude $f(\mathbf{k'},\mathbf{k})$ is given by:

$$f(\mathbf{k'},\mathbf{k}) = -\frac{1}{4\pi}(2\pi)^3\frac{2m}{\hbar^2}\langle \mathbf{k'}|V|\Psi^+\rangle \tag{2.16}$$

Where Ψ^+ is the outgoing spherical wave. It's useful to define the Transition Operator[15,17,18] $\hat{\mathbf{T}}$ such that:

$$V|\Psi\rangle = \hat{\mathbf{T}}|\Phi\rangle \tag{2.17}$$

The spherical symmetry of the potential V implies that $\hat{\mathbf{T}}$ commutes with both $\mathbf{L}$ and $\mathbf{L}^2$ (is a scalar operator). Expanding the amplitude $f(\mathbf{k'},\mathbf{k})$ in the spherical wave basis $|E,l,m\rangle$:

$$\begin{aligned} f(\mathbf{k'},\mathbf{k}) &= -\frac{1}{4\pi}(2\pi)^3\frac{2m}{\hbar^2}\langle \mathbf{k'}|\hat{\mathbf{T}}|\mathbf{k}\rangle \\ &= -\frac{1}{4\pi}(2\pi)^3\frac{2m}{\hbar^2}\sum_{l,m,l',m'}\int\int dEdE'\langle \mathbf{k'}|E',l',m'\rangle\langle E',l',m'|\hat{\mathbf{T}}|E,l,m\rangle\langle E,l,m|\mathbf{k}\rangle \\ &= -\frac{4\pi^2}{k}\sum_{l,m}T_l(E)\Big|_{E=\hbar^2k^2/2m} Y_l^m(\hat{\mathbf{k'}})Y_l^{m\dagger}(\hat{\mathbf{k}}) \end{aligned} \tag{2.18}$$

It is helpful here to define the parameter "partial-wave amplitude" $f_l(k)$ as follows:[17]

$$f_k(k) = -\frac{\pi T_l(E)}{k} \tag{2.19}$$

Now we can write:

$$f(\mathbf{k'},\mathbf{k}) = f(k,\theta) = \sum_{l=0}^{\infty}(2l+1)f_l(k)P_l(cos(\theta)) \tag{2.20}$$

Where P_l are the Legendre Polynomials. Now we can rewrite eq. 2.15 utilizing 2.20 and writing the plane wave as a sum of spherical waves[14] and we have (for large r):

$$\begin{aligned}\langle \mathbf{x}|\Psi\rangle &= \frac{1}{(2\pi)^{3/2}}\left[e^{ikz} + f(\theta)\frac{e^{ikr}}{r}\right] \\ &= \frac{1}{(2\pi)^{3/2}}\left[\sum_l (2l+1)P_l(cos(\theta))\frac{e^{ikr}-e^{-i(kr-l\pi)}}{2ikr} + \sum_l (2l+1)f_l(k)P_l(cos(\theta))\frac{e^{ikr}}{r}\right] \\ &= \frac{1}{(2\pi)^{3/2}}\sum_l (2l+1)\frac{P_l}{2ik}\left[[1+2ikf_l(k)]\frac{e^{ikr}}{r} - \frac{e^{-(kr-l\pi)}}{r}\right]\end{aligned} \tag{2.21}$$

Now we can begin to understand what is happening in the scattering process. In the absence of the scatterer, we have only a plane wave propagating, which can be written as a sum of spherical waves outgoing and incoming, as seen in eq. 2.21. The scatterer will only change the coefficient of the outgoing wave ($1 \to 1 + 2ikf_l(k)$) where the incoming wave remains unaffected.

Defining $S_l \equiv 1 + 2ikf_l(k)$ and observing in eq. 2.21 that it is changing the phase of the outgoing wave in the collision process, we can call it $S_l = e^{2\delta_l}$ ($2\delta_l$ is the phase where the factor 2 is conventional and δ_l is a function of k) and write[17]:

$$f_l = \frac{S_l - 1}{2ik} = \frac{e^{i\delta_l}sin(\delta_l)}{k} \tag{2.22}$$

We can rewrite eq. 2.20 for a different expression for $f(k,\theta)$:

$$f(k,\theta) = \frac{1}{k}\sum_{l=0}(2l+1)e^{i\delta_l}sin(\delta_l)P_l(cos(\theta)) \tag{2.23}$$

2.6 The scattering cross section

As seen in the previous section, a scattered wave can be written as a sum of a spherical wave going outwards the barrier and a term where is the original wave unaffected (equation 2.15). The scattering cross section will be the fraction of the original wave that

was scattered.[15] In order to obtain the cross section defined in eq. 2.6 we will look to the density flux $j(\mathbf{r})$ associated with the Schrödinger equation

$$\begin{aligned} j(\mathbf{r}) &= \frac{\hbar}{2mi}\left[\Psi^*(\mathbf{r})\nabla_r\Psi(\mathbf{r}) - \nabla_r\Psi^*(\mathbf{r})\Psi(\mathbf{r})\right] \\ &= Re\left[\frac{\hbar}{mi}\Psi^*(\mathbf{r})\nabla_r\Psi(\mathbf{r})\right] \end{aligned} \tag{2.24}$$

That satisfies the continuity equation:

$$\boldsymbol{\nabla}_{\boldsymbol{r}} \cdot \mathbf{j} + \frac{\partial \mid \Psi \mid^2}{\partial t} = 0 \tag{2.25}$$

Since we are considering to have a stationary system, we don‘t have a variation of the density with the time, so the equation reduces to:

$$\left[\frac{\partial}{\partial r}\hat{\mathbf{r}} + \frac{1}{r}\frac{\partial}{\partial\theta}\hat{\boldsymbol{\theta}} + \frac{1}{rsin\theta}\frac{\partial}{\partial\phi}\hat{\boldsymbol{\phi}}\right] \cdot \mathbf{j} = 0 \tag{2.26}$$

In spherical coordinates. The flux through a unit area of the incident wave vector $\mathbf{k}$ is given by:

$$\mathbf{j}_{\text{inc}} \cdot \hat{\mathbf{r}} = Re\left[A^*A\frac{\hbar}{mi}e^{-ikz}\frac{d}{dz}e^{ikz}\right] = A^* \cdot A \cdot v \tag{2.27}$$

The radial flux of the outgoing wave can be written as:

$$\begin{aligned} \mathbf{j}_{\text{out}} \cdot \hat{\mathbf{r}} &= Re\left[A^*A\frac{\hbar}{mi}f^*(\Omega)\frac{e^{-ikr}}{r}\frac{\partial}{\partial r}\left(f(\Omega)\frac{e^{ikr}}{r}\right)\right] \\ &= A^*Av\frac{\mid f(\Omega) \mid^2}{r^2} + \text{terms of higher order in 1/r} \end{aligned} \tag{2.28}$$

Now we can write, using the definition of cross section seen in section 1.2, the outgoing flux of particles passing through a spherical surface element $r^2d\Omega$ for large r, divided by the incident flux:

$$\frac{d\sigma}{d\Omega} = \mid f(\Omega) \mid^2 \tag{2.29}$$

Where $f(\Omega)$ is the amplitude of the scattered wave. We can write the total cross section:

$$\begin{aligned}\sigma_{Total} &= \int \mid f(k,\theta) \mid^2 d\Omega \\ &= \frac{1}{k^2}\int_0^{2\pi} d\phi \int_{-1}^{+1} d(cos(\theta)) \sum_l \sum_{l'} (2l+1)(2l'+1) e^{i\delta_l} sin(\delta_l) e^{-i\delta_{l'}} sin(\delta_{l'}) P_l P_{l'} \\ &= \frac{4\pi}{k^2}\sum_l (2l+1) sin^2(\delta_l)\end{aligned} \tag{2.30}$$

Now we can solve this equation for the total cross section for different types of particles:[15]

$$\begin{aligned}\text{For bosons: } \sigma_k &= \frac{8\pi}{k^2}\sum_{\text{l even}} (2l+1) sin^2(\delta_l(k)) \\ \text{For Fermions: } \sigma_k &= \frac{8\pi}{k^2}\sum_{\text{l odd}} (2l+1) sin^2(\delta_l(k)) \\ \text{For distinguishable particles: } \sigma_k &= \frac{4\pi}{k^2}\sum_{\text{all l}} (2l+1) sin^2(\delta_l(k))\end{aligned} \tag{2.31}$$

2.7 **Low energy limit:** s-wave scattering

At low temperatures (when 1/k is at least comparable with the range of the potential) terms of high order in l are not considered.[18] As seem on figure 4 we can see that classically atoms with l bigger than zero cannot penetrate the centrifugal barrier for such l. The effective potential for the l-th barrier is given by[18]:

$$V_{eff}(r) = V(r) + \frac{\hbar^2}{2\mu}\frac{l(l+1)}{r^2} \tag{2.32}$$

For system at low temperatures the collisions will be for the s-waves ($l = 0$). From equation 2.31 we can write the cross section for bosons with $l = 0$:

$$\sigma_0 = \frac{8\pi}{k^2} sin^2(\delta_0(k)) \tag{2.33}$$

We define the scattering length

$$a = \lim_{k\to 0} f_k = -\lim_{k\to 0}\frac{\delta_0(k)}{k} \tag{2.34}$$

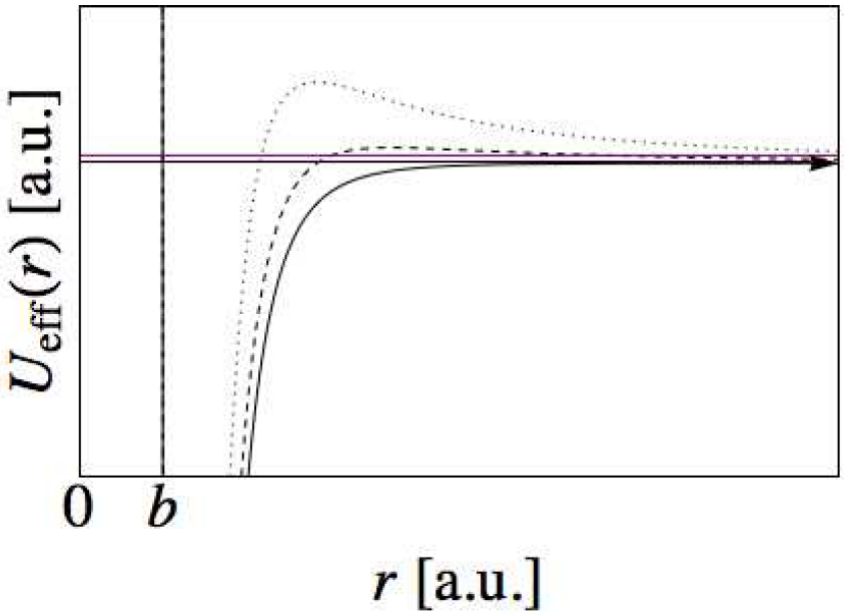

Figure 4 – The Van Der Waals potential in arbitrary units for l=0 (solid line), l=1 (dashed line) and l=2 (black dotted line). We can observe that the potential has a barrier at some point r=b where is extremely repulsive and for the l=0 the potential doesn't have a maximum and is attractive at long ranges, different from l=1 and l=2. The maximum creates a barrier where ultra cold gases cannot pass. This illustrates how only the l=0 part (s-wave) contributes to the problem.
Source: BENNO.[15]

The s-wave cross section is then depend only on the scattering length to first order:[15,18]

$$\sigma_0 = 8\pi a^2 \tag{2.35}$$

This parameter scattering length is quantifying the strength of the scattering. It is related to the phase gained in the collision and will be the only parameter necessary to characterize the interaction in the system.

2.8 The scattering length

As previously said, in an elastic collision between atoms at low temperatures, the atoms are like waves interacting. After the collision, the emergent waves are similar to those initially, but a phase δ was obtained, called the phase-shift (see figure 5). In this low-temperature regime, the acquired phase-shift and the momentum of the wave are related by:

$$\delta = -ka$$

The quantity "a" is called the scattering length and can be either positive or negative,

depending on the pair of atoms' interaction. This parameter is of great importance in cold atoms, being the only parameter necessary to characterize the system's interaction. Atoms repel when a is positive and attract when a is negative. Also, it adds a degree of control in the system since it is related to the interaction, and, as will be seen in the next chapter, it can be changed through a uniform magnetic field.

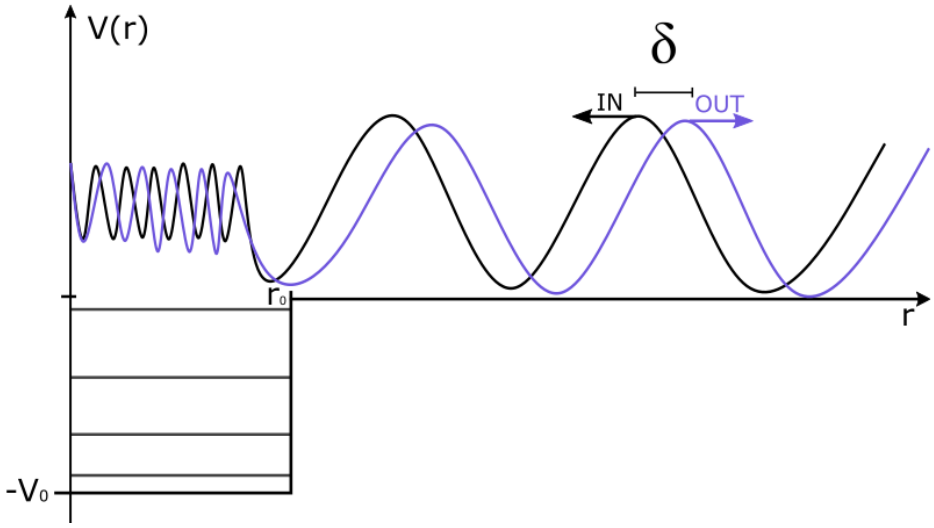

Figure 5 – The Phase-Shift acquired in the process of collision.
Source: By the author.

For different depths of the potential, the phase shift will differ as the atoms tend to expend more time together during specific depths (more in the next chapter). This leads to a different phase shift and, consequently, a different scattering length.

3 THE FESHBACH RESONANCES

This chapter will focus on the main topic of this dissertation: the Feshbach resonances (FR). We will talk about the different types of FR and other ways to tune them. The two channels model is used to explain the physics behind the resonances, and the square well simplification gives a good intuition behind the behavior near the points of resonance. We discuss effects customarily used to observe it experimentally and show the spectrum of resonances for our atomic species and its resonances with another alkali metal, the sodium. The reader can find a more detailed description of the Feshbach resonances and its various types in the work "Feshbach resonances in ultracold gases".[5]

3.1 Introduction

The Feshbach resonances were first introduced in the context of nuclear physics, used to explain the narrow resonances in the total cross section of a scattered neutron. In 1993 Boudewijn Verhaar proposed using this effect to manipulate the interaction in atomic quantum fluids[19] and only in 1998 the effect were observed, first by Inouye *et al.*[6] in an sodium BEC and in the same year by Courteille *et al.*[20] for ultracold rubidium atoms.This mechanism rapidly gained popularity in ultracold atoms, where the scattering length is of great importance as it controls the interaction, as shown in the last chapter.

Today this effect is well known and extensively used in cold atom physics wherein the presence of resonance the scattering length of the sample can go from $-\infty$ to ∞ allowing a high degree of control over the sample. This effect was observed by several groups[21–24] and has opened tons of possibilities. It can suppress the recombination in gases with negative or anomalous big scattering length, suppress three-body recombination in two-component Fermi gases, we can "turn off" the interaction to obtain a theoretical Bose-Einstein condensate, in addition to many others. With a two atomic mixture, the system becomes even richer with the possibility of altering the intra-species interaction and the inter-species, allowing all kinds of dynamics like different miscibility regimes,[2,25,26] molecule formation,[27,3,28] and more.[4]

3.2 The two channels model for Feshbach resonances

A Feshbach resonance is an effect involving multi-channels. In ultracold atoms, the channels are usually molecular potentials from a hyperfine manifold.[29] Nevertheless, the mechanism behind it can be understood by looking at the coupling between two channels in a collision, an open channel, and a closed channel (see section 2.1). The colliding particles interact in the open channel (or entrance channel) with a specific energy threshold E. Simultaneously, the pair of particles also have a closed channel that allows molecular states (bound states) but is inaccessible. Usually, each channel corresponds to different spin configurations and have different magnetic moments. By applying a homogeneous magnetic field, the channels will be dislocated by different amounts due to the different magnetic moments. So it is possible to change the relative position of the channels. This shifting can also be done by light; for more details, refer to Chin *et al.*[5]

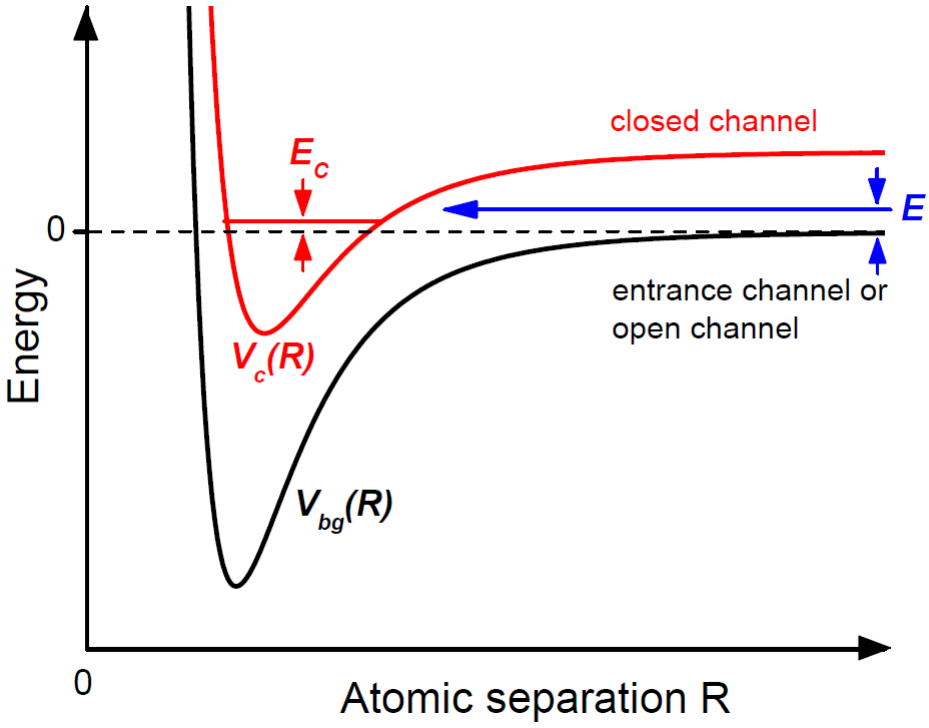

Figure 6 – Two channels model for the Feshbach resonances. The energy of a bound state in a closed channel (red curve) approach the threshold energy E in the entrance channel (black curve) by shifting the relative distance between the channels with a magnetic field.

Source: CHIN *et al.*.[5]

If the energy of the mentioned bound state gets close to the atoms' threshold energy in the entrance channel, they will stick together more during the collision, affecting the phase-shift and, consequently, the scattering length. Shifting the relative distance between

channels can bring the energy of one bound state closes to the threshold energy of the collision. This effect is known as the Feshbach resonances where the scattering length will diverge at the point of resonance. The following equation can describe the scattering length behaviour at the resonance.

$$a = a_{bg}\left(1 + \frac{\Delta}{B - B_0}\right) \tag{3.1}$$

where a_{bg} is the background scattering length, B_0 is the point of resonance and Δ is the width of the resonance (in Gauss), measured as the distance between the center of resonance and the point where the SL reaches zero. The coupling strength between the two channels will determine the width of the resonance,[15] where the better the coupling, the wider the Δ.

3.3 Modeling the interaction with a square well

In the previous section, we saw the two-channel model and its effects on the scattering length at the point of resonance. This section will focus on a intuitive way to see how a bound state affects the scattering length of a collision. By making a simple square well model, we can understand conceptually how the scattering length is changing. We will model the collision process with a simple "toy model" as called by Werner.[18] Landini also uses a similar approach in his thesis.[30] The model consists of a single potential that will illustrate the behaviour of the scattering length as the potential between particles begins to accommodate a bound-state. As we saw in the previous chapter, the scattering length relates to the phase gained in the collision approximately as:

$$\delta = -ak \tag{3.2}$$

For $R > b$ we can write the solution of the scattering as a sine wave

$$\Psi(r,t) \approx sin(kr + \delta) \approx k(r - a) \tag{3.3}$$

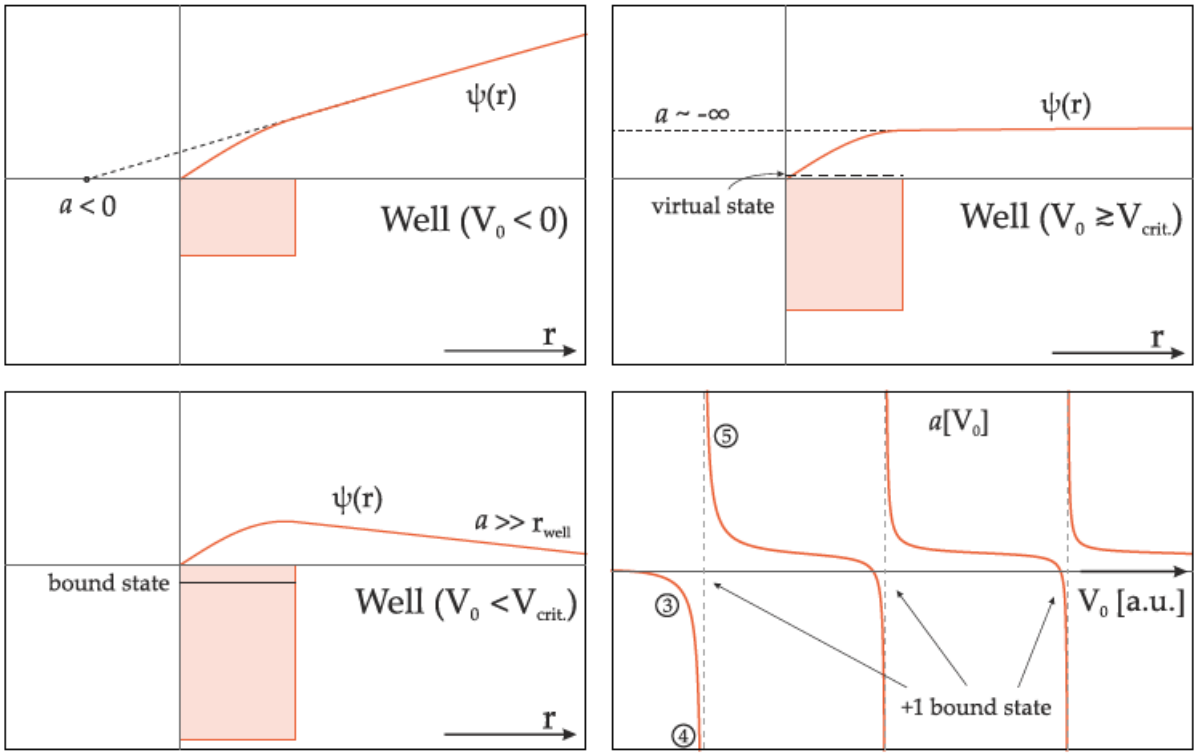

Figure 7 – Model to understand intuitively the changes and divergence of the scattering length close to a Feshbach resonance.
Source: Adapted from SCHULZE.[27]

We can easily tell the scattering length from this simple approximation by drawing a tangent line in the wavefunction's linear part. The point where it cross the x-axis will give the value of "a". If we have a square well with a depth of V_0 not deep enough to accommodate a bound-state, the tangent line will be somewhere in the negative spectrum. The moment the potential allows one bound state inside, the tangent line becomes parallel with the x-axis, giving $a = -\infty$. Making the potential a little deeper, the scattering length will pass from $-\infty$ to $+\infty$ and end up with a positive value.

This illustrates perfectly a Feshbach resonance, where we have control of the "deepness" of the potential shifting two internal states potential until a bound state becomes resonant with the entrance energy. There we have the divergence of the scattering length.

3.4 Observing a Feshbach resonance experimentally

This section will discuss how we can identify a Feshbach resonance experimentally and the signatures we should be looking for. There are several ways to do this experimentally,

and here we will talk about some of them. For more information, refer to Chin *et al.*[5] The most common way to characterize a resonance in cold atom experiments is by observing the inelastic losses at the points of resonance, where the three-body and twobody collisions are enhanced. This method has been used for measuring the Feshbach resonances experimentally for the first time in 1998 by Inouye *et al.*[6] where the resonance was observed by the enhancement of three-body losses in a Bose-Einstein condensate of sodium (figure 8) and still is a reliable form to observe the Feshbach resonances experimentally. We have selected this method to observe the resonances in our experiment.

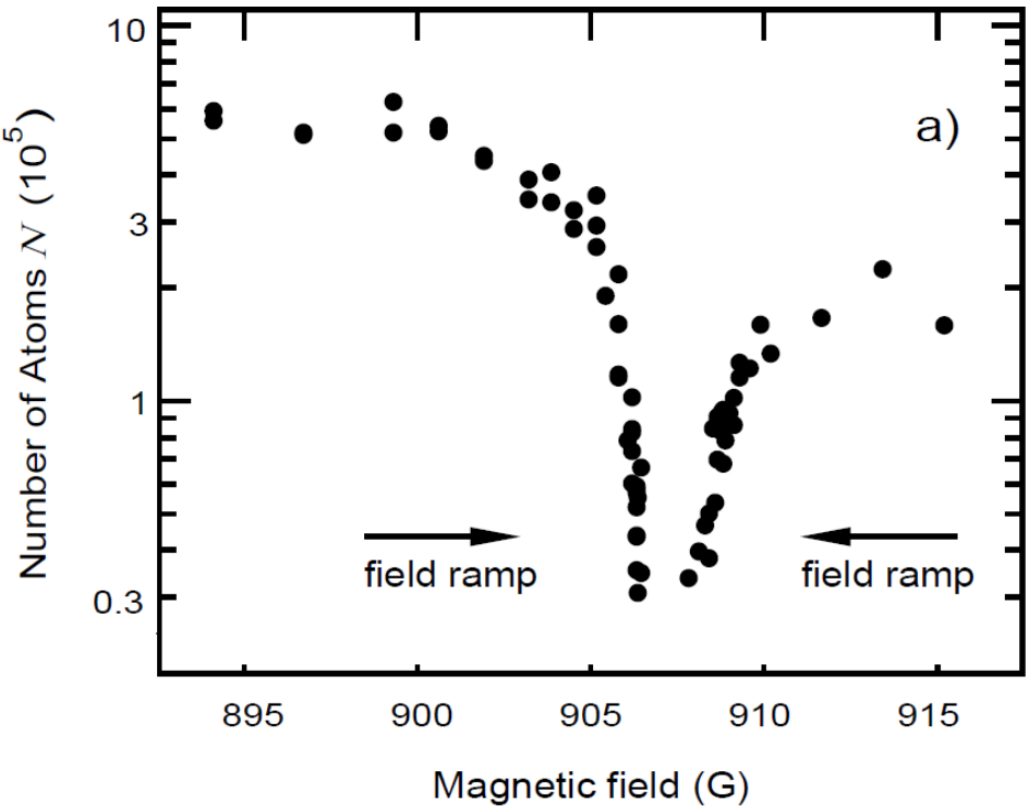

Figure 8 – Loss spectroscopy performed in a BEC of sodium in the first measurement of a Feshbach resonance experimentally.
Source: Adapted from INOUYE.[6]

The loss equation in a 3D harmonic trap at temperature T (considering that the thermalization occurs much faster than the inelastic losses) can be written as:

$$\frac{d\overline{n}(t)}{dt} = -\frac{\overline{n}(t)}{\tau} - L_2\overline{n}(t)^2 - (4/3)^{3/2}L_3\overline{n}(t)^3 \tag{3.4}$$

where the L_2 (L_3) is the thermally averaged two-body (three-body) loss coefficient, $\overline{n}(t)$ is the mean density and τ the one-body lifetime. At low temperatures is shown that the

three-body rate is proportional to the scattering length with $L_3 \propto a^4$.[19] Normally it is necessary a sufficient large density for this mechanism to be relevant as it is usually very small ($L_3 \sim 10^{-27} cm^6/s$).[29] But with the divergence of the scattering length, it becomes responsible for most of the losses near a resonance. The two-body process can also lead to a loss in the trap since the coefficient L_2 is enhanced near resonance, and at low temperatures, it takes a Lorentzian profile. These losses occur due to the release of the internal energy in the kinetic form in the collisional process, expelling the atoms from the trap. This release of energy near resonances also reflects in the temperature of the cloud, where near the resonances can also be observed an increase in the temperature.[31] A weakly dimer state can be achieved by performing a sweep over the resonance point to the side where the molecular level's energy is below the dissociation limit, a weakly dimer state can be archieved.[32] For the case of bosons, the atoms are quickly lost from the trap by inelastic atom-molecule and molecule-molecule collisions.[31]

The elastic collisions can also show evidence of a resonance. Due to the divergence of the scattering length, the cross-section of the system will increase drastically, enhancing the thermalization rate of the cloud. The scattering length can be tuned to zero in the same form, making $B = B_0 + \Delta$ in eq. 3.1, suppressing the collisions in the system. The lack of collisions will suppress the thermalization causing several losses when performing an evaporative cooling.

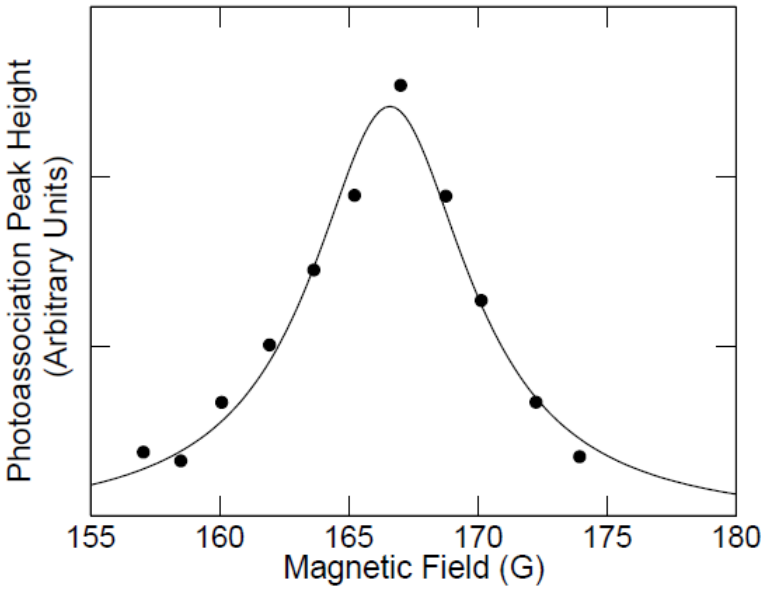

Figure 9 – Height of the photoassociation peaks as a function of the magnetic field revealing the Feshbach resonance.
Source: Adapted from COURTEILLE.[20]

One of the first observation of a Feshbach resonance in a cold atom system was done by Courteille *et al.*,[20] the Feshbach resonances were identified using radioative spectroscopy. This technique makes use of blue- or red-detuned light that induces losses by exciting atom pairs to an excited molecular state. Courteille *et al.* used a red-detuned beam fixed in the $S \rightarrow P$ transition in a experiment of ultracold rubidium atoms observing the height of the photoassociation near a resonance (see figure 9). In 2003, Chin *et al.*[28] used this technique with a blue-detuned beam in caesium samples.

3.5 The Feshbach resonances between 39K-39K and 23Na-39K

Our experiment aims to obtain a dual-species BEC of $^{23}Na -^{39} K$ with the aid of Feshbach resonances. Inter-species FR have been observed experimentally in the states $|1,-1\rangle$[33] and will be our reference for tuning the inter-species scattering length. Figure 10 shows both the inter and intra-species scattering length in the region of the resonances. The resonances show many possibilities with a region where the SL of sodium remains at $52a_0$ allowing a good collision rate and the condensation of the sample becomes possible. In the same region the inter-species interaction can be changed drastically allowing the study of the miscibility regimes, that will be talked more on the next section.

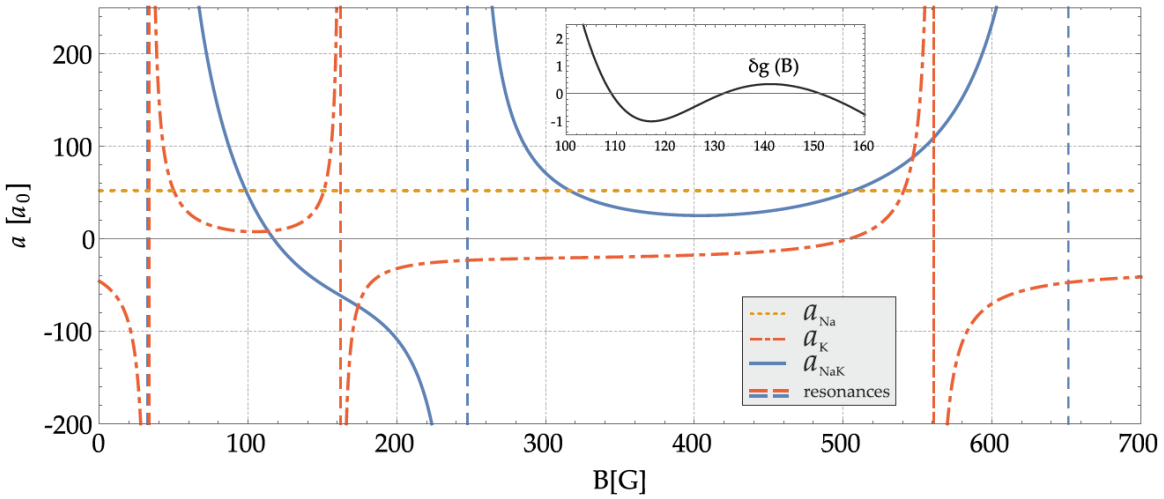

Figure 10 – The spectrum of Feshbach resonances between 23Na-39K (blue line), 23Na-23Na (dashed yellow line) and 39K-39K (dashed orange line) in the state $|1,-1\rangle$. The horizontal dashed lines represent the points of resonance. The little graphic indicates the range in which the miscibility between the species changes (see text).
Source: Adapted from SCHULZE.[33]

Since the sodium lasers were under maintenance at the time, this dissertation aims to characterize the intra-species Feshbach resonances for potassium 39 to prepare the

system for the dual-species experiment. This characterization will ensure the functionality of the system, where we can apply the technique mastered in a mixture of sodium and potassium. The theoretical calculated Feshbach resonances for potassium 39 in the $F = 1$ manifold are the following:

Table 1 – Theoretical values for the Feshbach resonances for potassium 39 in the F=1 manifold. The column B_0 corresponds to the point of each resonance and Δ the width.

m_F, m_F	B_0(G)	-Δ(G)
1,1	25.9	0.47
	402.4	52
	745.1	0.4
	752.4	0.4
0,0	58.8	9.6
	65.6	7.9
	471	72
	490	5
	825	0.032
	832	0.52
-1,-1	33.6	-55
	162.3	37
	560.7	56

Source: Adapted from D'ERRICO *et al.*[31]

Table 1 shows the points of each resonance along with the corresponding width, whose signal tells if the scattering length diverges to $-\infty$ or ∞ first. In Chapter 5 we present the resonances we have measured using loss spectroscopy for the pair $|F = 1, m_F = 0\rangle$

3.6 The miscibility regimes in a double mixture

A big attractive in this mixture is the possibility to tune the miscibility by changing the inter-species interaction.[2] We have two coupled equations in a double-condensate to describe the system's evolution, known as the coupled Gross-Pitaevskii equations:[34,35,7,27]

$$i\hbar\frac{\partial\Psi_i}{\partial t} = \left(\frac{-\hbar^2}{2m_i}\nabla^2 + V_i(r) + u_{ii} \mid \Psi_i(r,t) \mid^2 + u_{ij} \mid \Psi_j(r,t) \mid^2\right)\Psi_i(r,t) \tag{3.5}$$

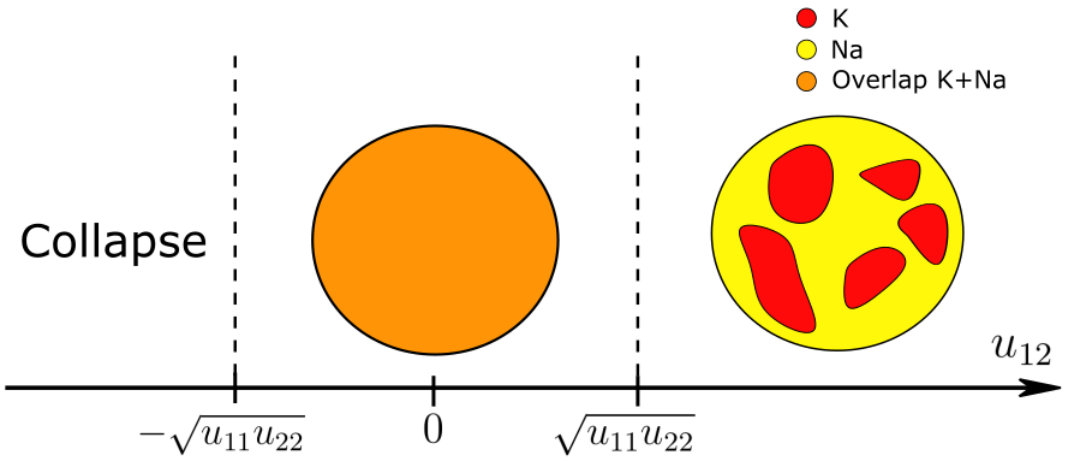

Figure 11 – An exemplification of the two miscibilities regimes a two specie mixture can have by altering the inter-species scattering length. In this image the distribution of one specie is shown in red and the other is shown in yellow, while the overlap of both species is shown in orange. By altering the u_{12} in respect to the u_{11} and u_{22} we can pass from a miscible regime to a immiscible. With a u_{12} negative enough the system will collapse.

Source: By the author.

Where the index $i, j = 1, 2$ correspond to the specie 1 and 2 with $i \neq j$. The $V_i(r)$ is the trapping potential for the specie i and the terms $u_{ii} = 4\pi\hbar^2 a_{ii}/m_i$, and $u_{ij} = 2\pi\hbar^2 a_{ij}/\mu_{ij}$ are the mean-field potentials, representing the strength of the intra-species and inter-specie interaction, respectively. The a_{ij} represent the scattering length of the specie i with the specie j, m_i is the mass of specie i and μ_{ij} is the reduced mass of the system. The mean-field terms can be controlled using Feshbach resonances, and for different set of parameters, we can expect different miscibility regimes, with the density distribution of the species overlapping (miscible regime) or being phase-separated (immiscible regime). The miscibility can by characterized by:

$$\delta g = u_{11}u_{22} - u_{12}^2 \tag{3.6}$$

When the interaction of one specie with itself is stronger than the inter-species interaction ($\delta g < 0$) then we have a immiscible regime, where the species begin to behave like water and oil, spatially separating the two components. Otherwise, if the interspecies term wins $\delta g > 0$, the system will be in the miscible regime. It's important to note that we need the intra-species SL to be always > 0 to prevent the collapse of the BECs. Even in this case, if the u_{ij} were set negative enough, the system will collapse as well. The

little graph in figure 10 represent the δg in function of the magnetic field. We see that between 100 G - 120 G we can explore the different miscibility regimes in the double superfluid mixture without collapsing the BECs (both a_{Na} and a_K are positive in this range). Miscibility effects have been observe in several BEC experiments[36,2,25,26] and will be explored in our experiment in the near future.

4 THE EXPERIMENTAL SETUP

In this section we will describe briefly the experimental apparatus necessary to obtain an ultra cold sample of potassium trapped in an optical trap and the instrumentation to tune the Feshbach resonances. A complete description can be found in the other thesis of the group [Castilho *et al.*,[7] Peñafiel *et al.*[9]] and also in our recent published paper [Castilho *et al.*[37]] where we describe the full apparatus for trapping both species.

Our system uses one program in Labview to generate the whole experimental sequence (shown in figure 23). This program sends the commands to a board from National Instruments that will control all the steps from the loading of the magneto-optical trap (MOT) to different steps as Gray Molasses (GM), Magnetic trap (MT), and ODT, allowing the condensation and its study using absorption imaging. In the Chapter 5 we will detail the sequence to trap the atoms in our optical trap and measure our first Feshbach resonance.

4.1 The vacuum chamber

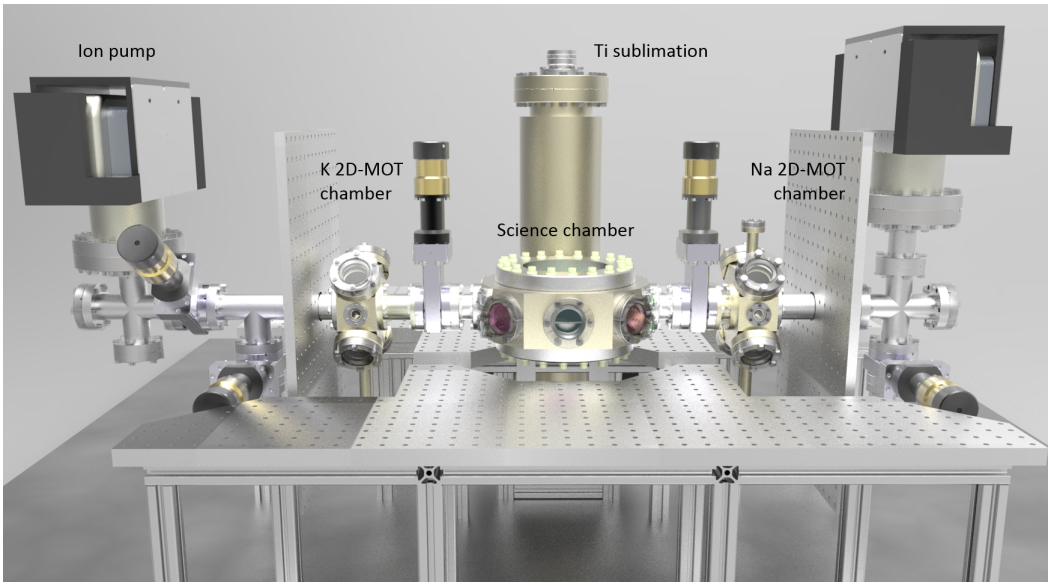

Figure 12 – The drawing of the vacuum system.
Source: CASTILHO.[7]

The vacuum system is probably the part that had changed the least over the time. Here we describe the main characteristics of our system and for more details the reader is advised to check the other thesis of the group.

Our vacuum system consists of three chambers, each being pumped by an ionic pump with pressures below 10^{-9} Torr. The two side chambers are directly above the atomic oven for each specie (see figure 12). The oven provides an atomic beam into each side chamber where the atoms are trapped in two-dimensional magneto optical traps (2D MOTs), where the configuration was inspired by the work in.[38] The K oven is set at 120 °C and is connected to a timer programmed to turn on each day two hours before we arrive at the laboratory, ensuring a good atom flux at the beginning of the day.

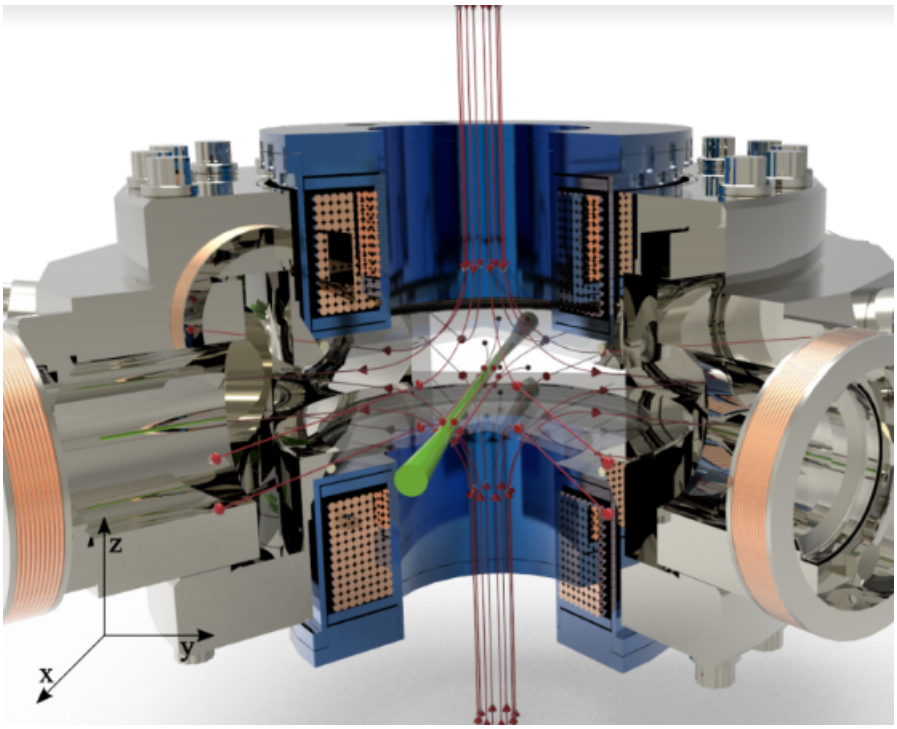

Figure 13 – Sectional view of the Science Chamber.
Source: By the author.

Both side chambers are connected to a central chamber (the Science Chamber) by gate valves. An atomic flux coming from the 2D chambers enter in the SC though the differential pumping tubes, this configuration allows a lower pressure in the SC ensuring a good lifetime of the atoms in our trap. The atoms are first loaded in a 2D MOT and are pushed to the main chamber through a red-detuned beam called the "push" beam. Once in the Science Chamber, the atoms are trapped by three counter propagating beams in a region with a quadrupolar magnetic field provided by the pair of coil in anti-Helmholtz configuration (the 3D MOT). The pair of coils (the Quadrupole/Feshbach Coils) are protected by a case that allows a constant flux of cold water to flow and prevent excessive heating. This case is coupled to the main chamber maintaining the pair of coils close to

anti-Helmholtz configuration. For fine adjustment of the magnetic field we have three pair of little compensation coils allowing us full spatial control of the point of zero field.

4.2 The laser system for 39K

We have three lasers for potassium, two for the D2 transition (one for each Cooling and Repumper transition) and one for the D1 transition. A closed cooling transition is made in the D2 line where the cooling frequency ($|F = 2\rangle \rightarrow |F' = 3\rangle$) provides a molasses region for the MOTs and the Repumper frequency ($|F = 1\rangle \rightarrow |F' = 2\rangle$) ensures that the atoms stays in the cycle. One difficulty we have with the potassium specie is the separation between the hyperfine states in the D_2 line (38.8 MHz for 39K), so in order to maintain a closed transition is needed more repumper light. The D1 transition is necessary for the Compressed MOT hybrid and for the Gray Molasses stage,,[39] the latter is where the sample is cooled below the doppler limit. A dissertation focusing on the Gray Molasses stage is being written by our master student Edward Iraita and will be available soon. The natural line width is 6.035 MHz for the D2 transition and 5.956 MHz for the D1 transition. The frequencies used in the experiment and their respective locking points are illustrated in figure 14.

For a each transition (D_2 and D_1) we lock our frequencies based on the dispersion signal obtained by the saturated absorption technique. In a potassium vapour cell containing the atomic sample, we input two counter-propagating beams named pump beam and probe beam. The pump beam has a higher intensity and will saturate the transition for the atoms within a certain group velocity (the atoms won't be able to absorb more light). On the other hand, the probe beam will excite another group velocity due to the doppler effect, but will see a "hole" associated with the atoms absorbing the pump beam that could also can absorb the probe beam. These atoms have its velocity close to zero along the direction of propagation of the beams and are a good reference for the transition. The signal is collected by a fast photodetector, which send the absorption signal to the Digilock module by Toptica. With the signal we generate a dispersion and lock the laser in frequency, from the ground state crossover to the 1st excited state crossover.

Since the atoms require a lot of power due to the small hyperfine splitting, it was necessary to build two homemade Master Oscillator Power Amplifier (MOPA),[7] with this, the light is amplified before injecting it into the optical fibers that guides light to the

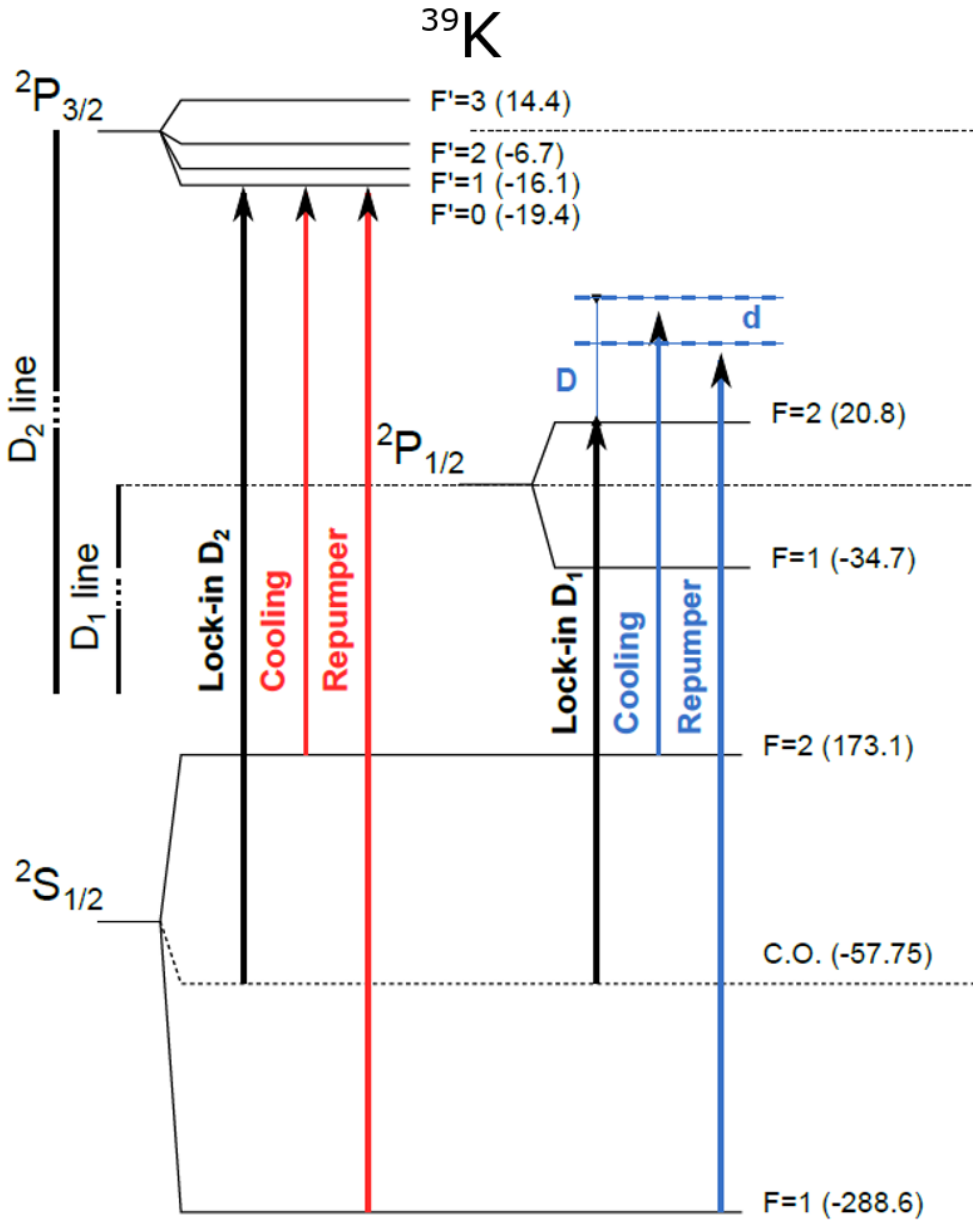

Figure 14 – Frequency scheme for potassium 39.
Source: Adapted from CASTILHO.[7]

vacuum chamber. We use one MOPA for the 2D MOT (called 2D MOPA) and another for the 3D MOT (3D MOPA) where is injected a total of 45 mW summing the Cooling and Repumper light. The input ratio can be controlled by a wave plate right before the MOPA and we can see the output ratio on a Fabry-Perot cavity where we inject a little of the 3D light. The ratio is optimized in the waveplate choosing the value that enhances the MOT signal of fluorescence. Coming out of the optical fiber we have 310 mW of the 3D light and around 300 mW of 2D light. In the stage of Gray Molasses when the D2 light is turned off the D1 light is injected in the MOPA 3D for a output power of 310 mW. Table

2 shows the power and frequency of the light used in the MOT stage. For the push beam we use the light from the 2D MOT with a power of 300 μW.

Table 2 – Light detuning and power for the MOT stage

Light	Detuning (MHz)	Power (mW)
Repumper 3D	-36	50
Cooling 3D	-31	260
Cooling 2D	-21	150
Repumper 2D	-18	150

Source: By the author.

Since there is the possibility to work with another potassium isotope (the potassium 41) we build the absorption system able to rapidly switch between the isotopes. We built two tracks the beam can travel with Acoustic Optical Modulators - AOMs set at different frequencies. Using a waveplate we can quickly switch the tracks, transitioning the absorption signal from one isotope to the other if needed.

4.3 The Optical Dipole Trap setup

In order to explore the properties of interaction tuning in both atomic species, together and individually, we need to change to a pure optical trap. In the first stage of the experiment we use the well known MOT technique, which combines a magnetic field in anti-Helmholtz configuration with three red detuned counter propagating beams. This technique allow us to confine the atoms in a small region of space (in the order of 1 mm) with a number of approximately 10^8 atoms of potassium and 7×10^9 atoms of sodium in our experiment.

However, the Feshbach resonances technique utilizes a uniform magnetic field, that is not compatible with the gradient used in the MOT. For this reason we need to transfer the atoms to an Optical Dipole Trap.[7,40] This kind of trap can confine neutral atoms by purely optical means and is a indispensable tool for our purposes.

An atom placed in a focused laser beam will obtain a induced dipole moment $\vec{p}(t) = \alpha\vec{E}(t)$ caused by the electric field of the light, with α being the complex polarizability of the atom. The potential describing the interaction of this induced dipole with the electric

field can be written (under certain coditions) as:[40]

$$V_{Dip} = \frac{3\pi c^2}{2\omega_0^3}\left(\frac{\Gamma}{\Delta}\right) I(\vec{r}) \tag{4.1}$$

Where c is the speed of light, ω_0 is the angular frequency of the atomic transition, Δ is the detuning between the laser beam and the atomic transition, $I(r)$ is the intensity profile and Γ is the resonant damping rate. For a red-detuned beam ($\Delta < 0$) this potential will have it's minimum at the focus point, where the confining will take place. One disadvantage of this type of trap is the necessity of high intensity since the usual depths are very shallow (a few 10 μK deep).

In the case of a focusing Gaussian beam propagating in the x direction, we can write the expression for $I(r, x)$:

$$I(r, x) = \frac{2P}{\pi w_0^2(1 + (x/x_r)^2)} exp\left(\frac{-2r^2}{w_0^2(1 + (x/x_r)^2)}\right) \tag{4.2}$$

Where P is the power of the laser, w_0 is the radius at the focus (called the beam waist), r is the radial profile and $x_r = \pi w_0^2/\lambda$ is the Rayleigh length of our laser, the length along the propagating axis where our beam radius increases from w_0 to $\sqrt{2}w_0$. Our configuration uses two orthogonal beams (propagating along the x and y direction) crossing at the focus point: the center of our trap. The expression then becomes

$$V_{Dip} = \frac{3\pi c^2}{2\omega_0^3}\left(\frac{\Gamma}{\Delta}\right)(I_1(x, y, z) + I_2(x, y, z)) \tag{4.3}$$

with I_i, $i = 1, 2$ the intensity of each beam described in equation 4.2. By performing the harmonical approximation we can write this expression as[41]

$$V(x, y, z) \simeq \frac{3c^2\Gamma}{\omega_0^3\Delta}\left(\frac{P_1}{w_1^2} + \frac{P_2}{w_2^2}\right) + \frac{m}{2}(x^2\omega_x^2 + y^2\omega_y^2 + z^2\omega_z^2) \tag{4.4}$$

The index 1,2 refer to each arm and the terms $(\omega_x, \omega_y, \omega_z)$ are the frequencies of the ODT in each direction.

The laser used for the optical trap in our experiment is a MEPHISTO laser, capable of generating 42 W of light at the wavelength of 1064 nm (far red-detuned). The light goes past an isolator (that prevents any light from coming back) and is divided into two ways,

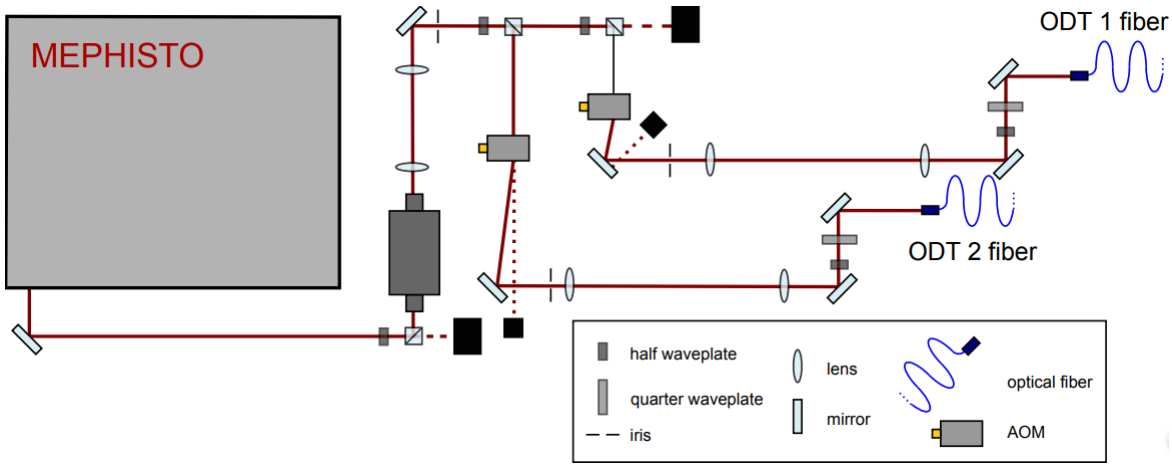

Figure 15 – Schematic of the ODT Laser system.
Source: Adapted from CASTILHO.[7]

each designed to be one arm of the trap. Each arm has an AOM necessary to switch the light on and off during the experiment and is coupled to an optical fiber. The configuration of the trap in the SC was improved by making the crossed trap with only one arm (figure 16) improving the total power in the atoms from 10 W to around 20 W. From which direction the beam is injected can be chosen by a rotating a wave plate before our beam splitter (figure 15). After the first beam exits the chamber it encounters a waveplate that either allows the beam to re-enter the chamber or send it to a beam stop. We lost the ability to control the arms separately but the gain in depth was worth it. We used this control in our attempt to "clean" the spin in the sample, leaving only one state of the $|F = 1\rangle$ manifold in the trap, discussed later in the results.

The control over the beams also helps in the alignment process, where we first optimize the number of atoms trapped using one arm then we overlap the first beam with the second beam and improve the density again. The laser also have a PID system for power stability in the trap preventing eventual fluctuations that could lead to atom loss. The waist of each beam in the center is 80 µm and our trap have the depth of around 130 μK. To transfer a good portion of the atoms to the ODT, the depth is necessary to be at least ten times deeper than the actual temperature of the cloud. Since our atoms are around 12 μK at the end of the cooling process we managed to obtain a reasonable atom number in our ODT.

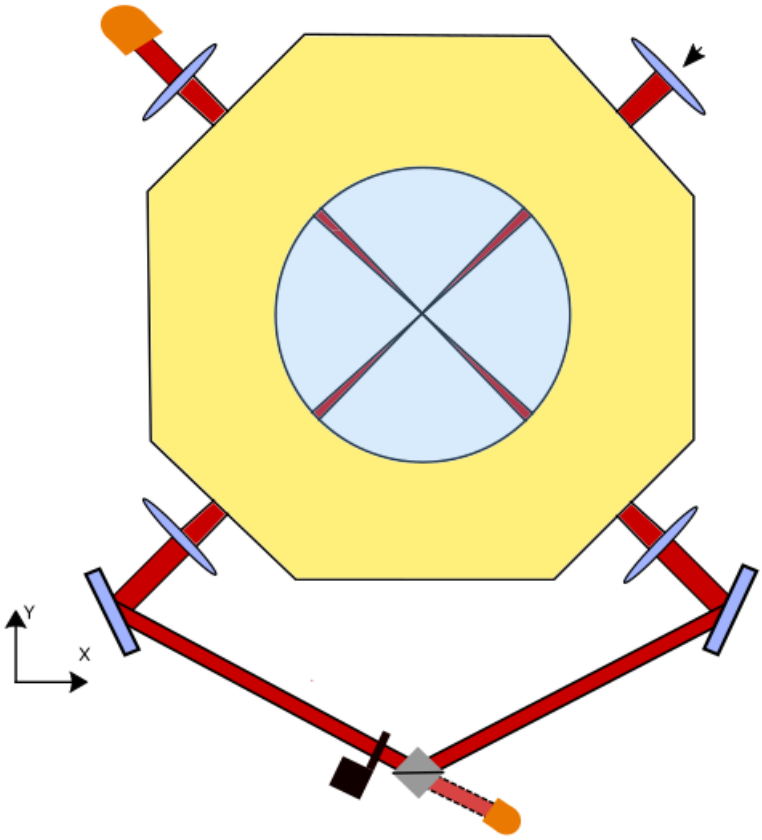

Figure 16 – ODT system in the Science Chamber as seem from above. A single beam is focused in the center of the chamber before exiting to re-enter crosswise. We use a little motor (black square in the figure) capable to rotate a birefringent blade before a beam splitter (gray square).
Source: By the author.

4.4 Tuning the Feshbach resonances

Usually, in order to tune the interaction via Feshbach resonances, a high homogeneous magnetic field is necessary. The spectrum of the potassium resonances we would like to study ranges from a few Gauss to 800 Gauss (see table 1). In many other experiments, additional coils are implemented for that purpose. In our case we have decided to use the H-Bridge technique,[35,42,43] where we can have our coils in anti-Helmholtz configuration for the MOT and Magnetic Trap stages, and switch them to the Helmholtz configuration, making it possible to scan a uniform magnetic field to access the FR, using the same pair of coils. Next the quadrupole coils system is detailed with its specifications and the system implemented to switch from anti-Helmholtz to Helmholtz configuration is shown.

4.4.1 The quadrupole/Feshbach coils

As mentioned before, the coils responsible for the quadrupole field in our MOT will be the same used to tune the Feshbach resonances. The coils are placed in a hollow Delrin support that allows a constant flux of water provided by a chiller at 11 degrees Celsius. Each coil have an internal radius of 40.4 mm, an inductance of 1.7 mF and were made with 10 layers of 16 loops of insulated copper wire of 2.18 mm diameter. Each coil has a resistance of 0.35 Ω and are both placed at 62 mm from each other. In figure 17 (left) we show the pair of coils inside the support placed for magnetic field characterization, where the field orientation is in anti-Helmholtz configuration while on the right we have the coils inserted in the Science Chamber, where we have re-entrant windows allowing the good proximity of the coils.

Inside the support we also have a pair of little coils that can be controlled independently and are used as a compensation field, only capable of translating a little the center of the quadrupole. The pair of compensation coils are powered by a font lambda and controlled by a IGBT. The field is directed upwards to agree with the future Feshbach field and it generates a field of around 1 G in the region of the cloud during the time we choose on our time sequence.

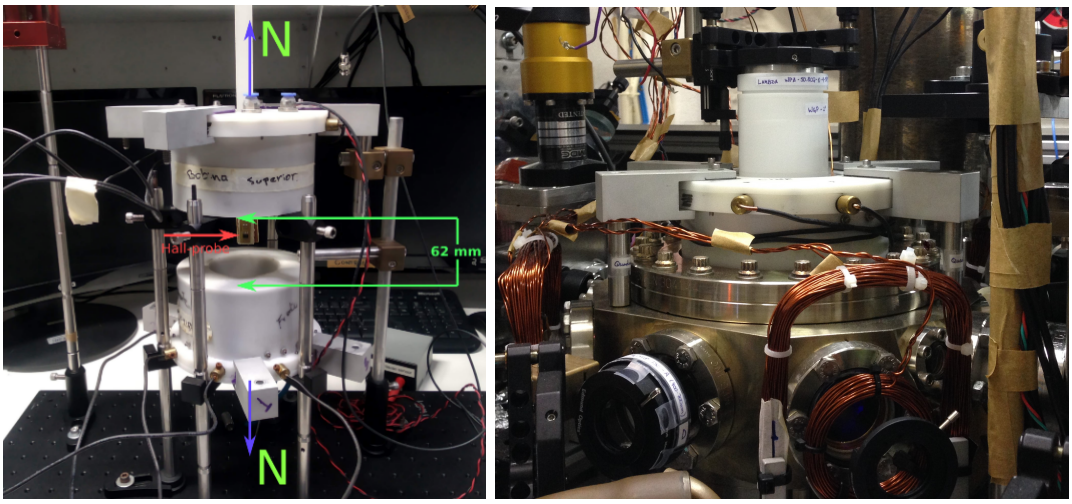

Figure 17 – Quadrupole coils installed outside the system for field characterization (left) and the coils coupled in the Science Chamber (right).
Source: By the author.

The quadrupole coils are in a anti-Helmholtz configuration with the field orientation shown in figure 17. The H-bridge is installed in the bottom coil where the direction of the electric current will be switched (more on the next section) and we will obtain a Helmholtz

configuration. The calibration for both regimes are the following:

$$\frac{dB_{Quad}}{dz}(z \simeq 0) = I \cdot 5.34G/A \cdot cm \tag{4.5}$$

$$B_{Fesh}(z = 0) = I \cdot 16.07G/A \tag{4.6}$$

Using the package Radia in the Mathematica software we were capable of simulating our system of coils we obtained a good agreement between the simulation and the measurement done with a hall probe (figure 18). We have the power supplier Delta Elektronika SM 120-50 controlled by an analogical signal, and the switching process provided by IGBTs (SKM150GB12T4) controlled by digital signals. All analogical and digital signals are provided by a National Instruments installed in a computer, and those signals are controlled by a program made in LabView. All this instrumentation makes possible a time sequence for different situations in the experiment, as mentioned before.

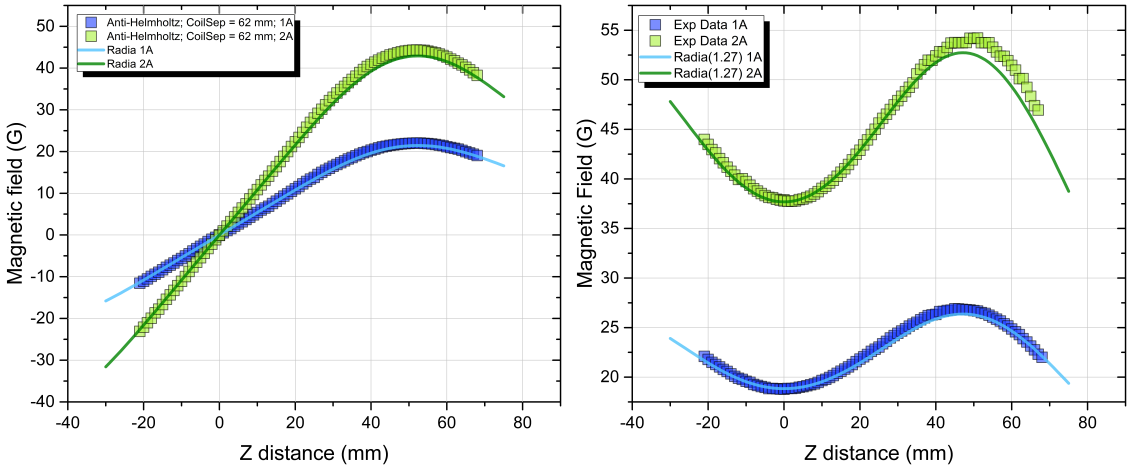

Figure 18 – On the left (right) we have the plot of the magnetic field obtained by the simulation done using the Radia package on Mathematica and the measurement along the z axis using a Hall probe for two different currents in anti-Helmholtz (Helmholtz) configuration.

Source: By the author.

With this system we are able to obtain a homogeneous magnetic field in the region of the atoms of around 1000 G, more than enough to explore the whole spectrum of Feshbach resonances in any of the $F = 1$ manifold (table 1) and also, the interspecies resonances between sodium and potassium in the $|1, -1\rangle$ state (figure 10). In the next section we will describe the H-Bridge, the apparatus necessary for the switch of current during the experiment.

4.4.2 The control system for the H-bridge

As mentioned before, by simply inverting the orientation of the current in one of the coils, we can switch the coils configuration from anti-Helmlholtz to Helmholtz, where we have a uniform field in the region of the atoms. For this purpose we installed an H-Bridge system. In the Figure 19, we have a sketch of the H-bridge, showing the switch in the orientation of the current in one of our coils, where L and R represent the inductance and resistance, respectively, both associated with our coil. A power circuit enables the current to circulate as indicated for each configuration, illustrated in the left and right of figure 19. This is possible because we have controlled four power switches, named as C1, C2, C3 and C4, which are turned on and off alternately, as indicated, to guarantee each situation in the appropriate step of the experiment. Those power switches are IGBTs, as the ones mentioned before. Our H-Bridge system was assembled and tested by the undergrad student Guilherme Neto.

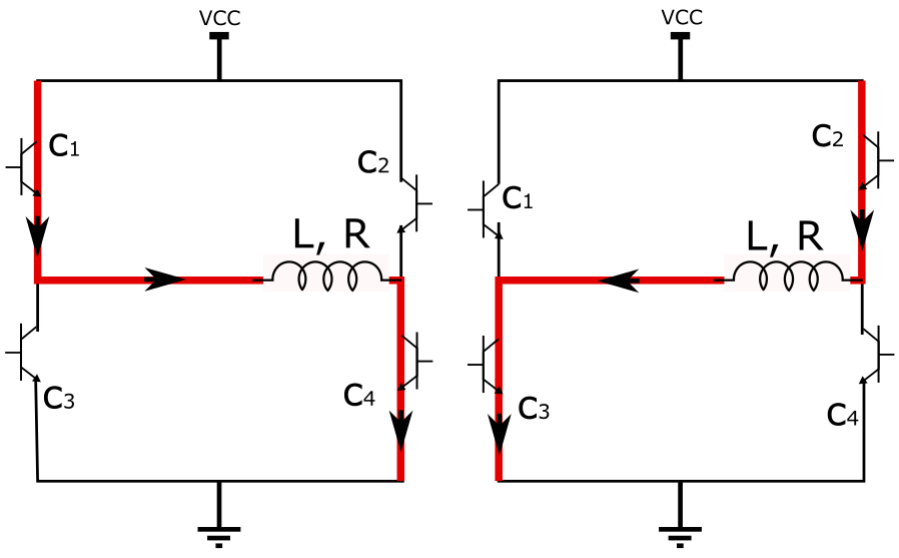

Figure 19 – Schematic figure of the H-Bridge system.
Source: By the author.

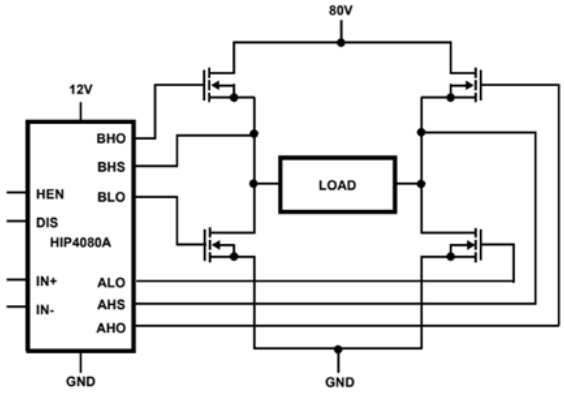

Figure 20 – Block diagram of the chip HIP4080A used in the control of the H-Bridge.
Source: By the author.

For the electronic control we use a chip [HIP 4080A] that serves as a driver for the power IGBTs [SKM150GB12T4]. Using a digital signal from our National board, we have choose which pair of IGBT is open or closed. When we send 5 V to the IGBT driver, it opens the C1 and C4 IGBTs and closes the C2 and C3, and when we send 0 V is the other way around. By this command we can easily change from one configuration to another. One important feature of the driver HIP 4080A is that when eventually when the power supply is neither 0 V or 5 V, but in between, all the gates are open, to secure that we don't have any current in the system. We observed that this method of switching OFF the current was faster than any other configuration tried before. We modified the system to use this as the turn OFF method. Figure 20 shows the application block diagram for the full bridge chip HIP4080A used in the control.

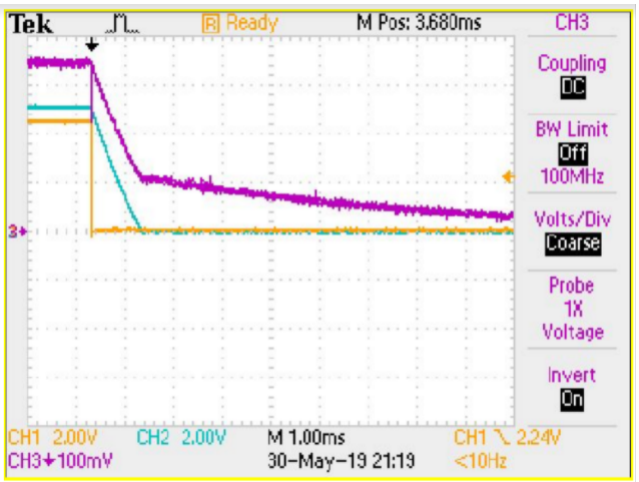

Figure 21 – Test of the turning OFF of the magnetic field by the IGBT in the H-Bridge system. The orange curve corresponds to the oscilloscope, the blue curve to the transducer and the purple curve to the hall probe.
Source: By the author.

The H-Bridge system were tested several times before finally being inserted in the experiment. We have used hall probes and transducers [IT 200-S ULTRASTAB from LEM] to monitor the current circulating in the circuit. In figure 21 we present the signals showing how fast was the turning OFF of the magnetic field in the Helmholtz configuration. We applied 51 A to the coils that was abruptly turned OFF. The digital signal used for that is the channel 1 in the oscilloscope (orange line). We can see from the other channels (channel 2 for the transducer and channel 3 for the hall probe) that the falling time is close to 1 ms. This is considered a good transient time considering the regular TOFs we use for imaging

4.5 The image table

Next to the Science Chamber we have our image table for the horizontal image where we have installed our Stingray CCDs. The table was built in a configuration were the light can go through two paths, with different magnifications each, before reaching the CCD (see image 22). This configuration is very useful because in different stages of the experiment we need to have a good resolution on sizes from 1 mm (MOT) to 50 μm (ODT) where we would lack the resolution necessary to diagnose the image. The image beam is magnified once it exits the Science Chamber and will follow one of the two paths ahead, depending if the removable mirror is placed. On path number 1 we have the magnification of 1.66 and the image from the atoms is focused on the CCD, 250 mm away from the last lens. On path number 2 the light is demagnified to 0.5 before reaching the CCD, 60 mm away from the last lens.

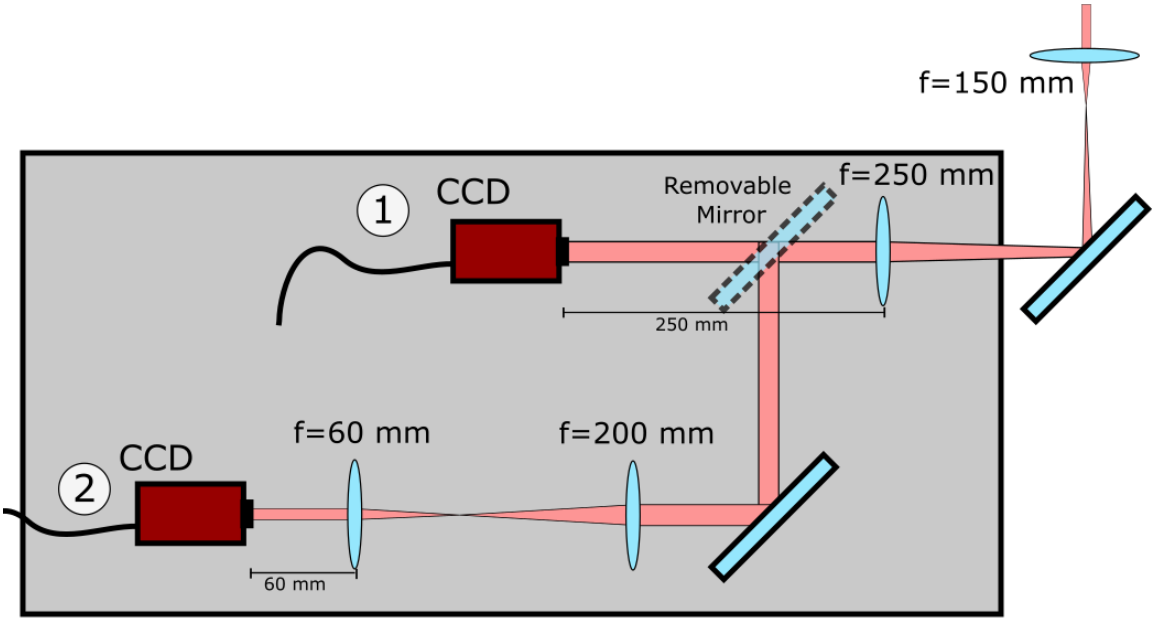

Figure 22 – Configuration of the image table. There we can choose between two magnifications to observe our atomic cloud in the horizontal plane. The beam is magnified after exiting the Science Chamber and is demagnified on path number 2. With the CCD on 1 (2) we have a magnification of 1.66 (0.5).
Source: By the author.

Our imaging system consists on the Absorption Imaging Technique, where we shine a resonant beam into the atoms (light that is later captured by the CCD) and take three pictures: In the first one, the beam pass through the atoms, which absorbs the resonant light. The second one is taken without the atoms, and the third picture is taken without the resonant light, only background noise. After normalizing the image we can obtain the density profile of our cloud by the Beer-Lambert law, that relates the intensity of a beam propagating in a certain direction with the density of the medium[29,7]:

$$I(x,y) = I_0(x,y)e^{-\Lambda \int n(x,y,z)dz} \tag{4.7}$$

Where $I_0(x,y)$ is the intensity of the beam before entering the medium (propagating in the z direction), Λ is the transversal section of absorption and $n(x,y,z)$ the density of the medium. From this equation we can obtain our density profile:

$$\rho(x,y) = \int n(x,y)dz = \frac{-1}{\Lambda} ln \frac{I(x,y)}{I_0(x,y)} \tag{4.8}$$

By performing this integration we obtain our atom number. The temperature of the cloud can be obtained by the "Time of Flight - TOF" technique, where the trap is turned OFF

and the atoms fall freely for a certain time (called the TOF) before we take the picture. By performing this for two different TOFs we can analyse how the cloud expand in that time and extract the temperature form there. After the pictures are normalized we use a program written in Python to fit the density profile by a Gaussian for the classic gas expanding or by a bimodal fit for the BEC.

5 FIRST RESULTS AND DISCUSSION

In this chapter will be discussed the process of obtaining a reasonable amount of potassium atoms trapped in a pure optical trap and the method used for tuning the Feshbach resonances in the state $|F = 1, m_F = 0\rangle$. The first step towards the scanning of the resonances is the cooling sequence, since our optical potential is very shallow (130 μK) and we need the sample ten times cooler than that for a good transferring. Some steps of the sequence had the objective to clean the spin because we originally wanted to leave only the $m_F = -1$. The whole sequence will be shown with the experimental numbers we obtained with the difficulty encountered along the way.

5.1 The cooling and trapping sequence for K

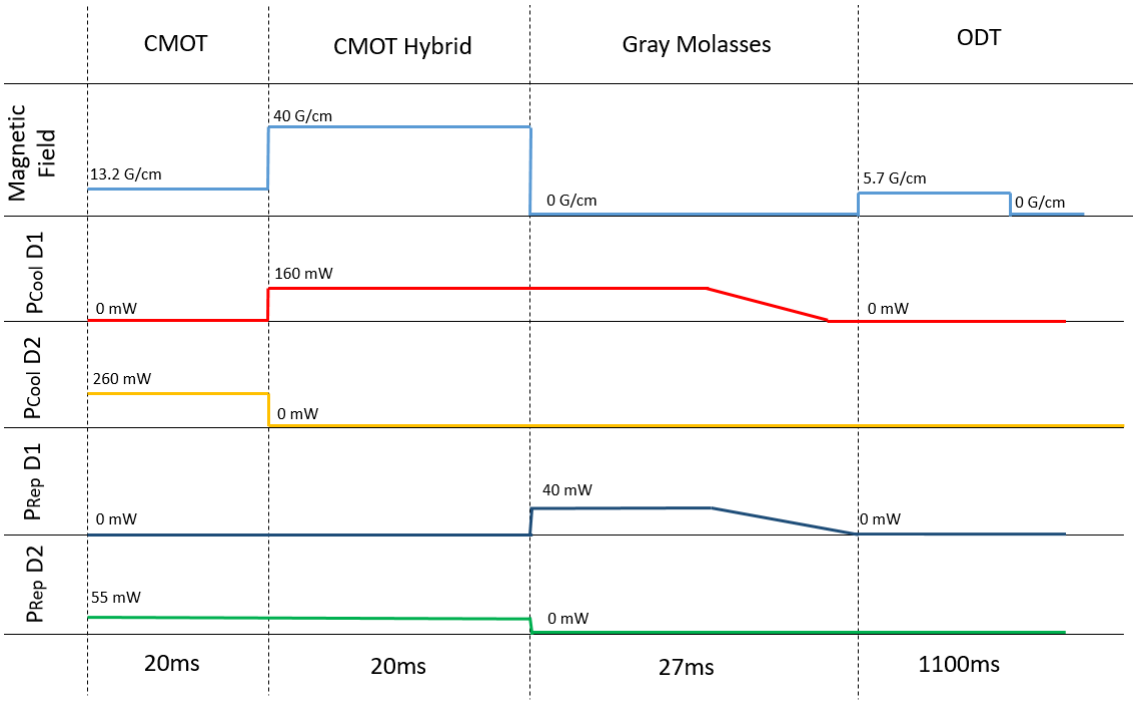

Figure 23 – Experimental sequence with the magnetic field and light of each step.
Source: By the author.

The experimental sequence is illustrated in 23. We begin the sequence loading the potassium atoms in our 3D MOT for 12 seconds, where we obtain 10^8 potassium atoms trapped at the temperature of 5 mK. At this stage, our magnetic field is a linear gradient of approximately 11 G/cm, and we have the same amount of Cooling and Repumper light where little adjusts are made to optimize the MOT signal of fluorescence. After loading

the MOT to maximum number, the real sequence occurs. First we have a "Compressed MOT - CMOT" stage where the gradient increases, and the frequencies are changed lightly. The next step is also a Compressed MOT stage, but it makes use of both D1 and D2 light. This stage is called CMOT Hybrid and we use the D1 line on the Cooling transition and the D2 line on the Repumper transition. This configuration allows us to obtain a even lower temperature. At the end of this stage we have around 7×10^7 atoms at the temperature of 700 μK.

The next stage is the responsible for the highest increase in the PSD in our experiment and is known as the Gray Molasses.[39] At zero magnetic field and using the D1 transition, the gray molasses use velocity selective coherent population trapping (VSCPT) and Sisyphus Cooling to cool the atoms bellow the Doppler limit. A full dissertation is being written about this process by our master student Edward Iraita where the theory and a more profound discussion will be found. At this stage, the magnetic field is turned off, and the D1 light is injected in the 3D MOPA, where it is amplified and send to the SC, where a total of 300 mW is divided in the MOT beams. For maximum cooling efficiency, it was observed that lowering the intensity of the beams during this stage accomplishes an even lower temperature for potassium 39.[39] By lowering the intensity, we could go from 70 μK to 12 μK. These stages go on for 15 ms and a good image of our atomic cloud can finally be observed, where we have measured around 12 μK as mentioned before.

The next step is transfer the atomic cloud to the Optical Dipole Trap, where the Feshbach scan will occur. There are two most important aspects in this transference. A good mode matching between the atomic cloud and the ODT is necessary for an efficient transfer; a discrepancy between the sizes will result in losing a big part of the atomic cloud during the transfer. The temperature of our cloud is another important aspect where we need a mean temperature which is ten times lower than the potential depth, that is already shallow, in order to trap a suitable amount of the atoms. We thought of two ways of proceeding: we could either send the atoms to a pure magnetic trap before transferring to the ODT or we could send them directly from the gray molasses stage.

Opting for the magnetic trap stage will improve the mode matching since the MT is highly confining. The MT can also "clean" the spin of the sample (leaving only one m_F state), since for low fields only the $|F = 1, m_F = -1\rangle$ is low field-seeking, repelling the $|m_F = 1\rangle$ while the $m_F = 0$ falls from the trap.

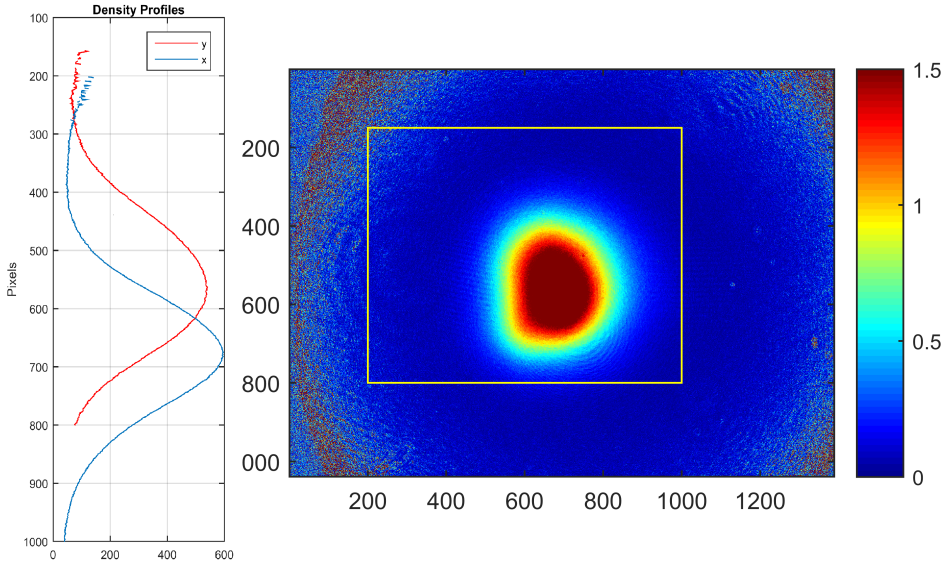

Figure 24 – Absorption image obtained after the gray molasses. The atoms were expanding freely for 10 ms. On the left we have the density profiles on the x direction (y direction) in blue (red).

Source: By the author.

The downside is that the process of transferring the atoms to the MT can be very perturbative, heating the cloud considerably. Ideally, with the sodium ready, we could transfer both species to the MT and perform an evaporative cooling on sodium using microwave. Then the sodium can be used as a coolant for potassium in the MT before being transferred to the ODT. Since the sodium was not available during this work, the best method was transferring directly from the gray molasses.

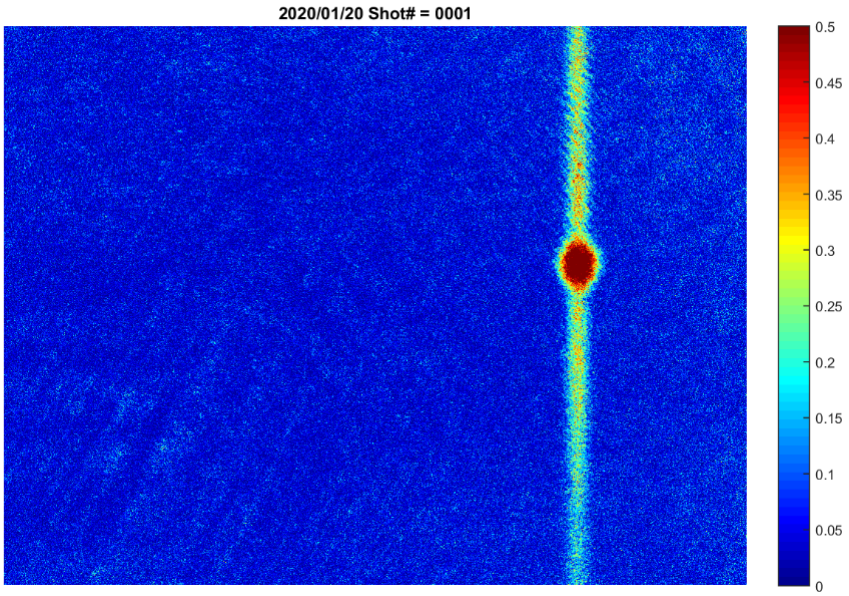

Figure 25 – A horizontal image of the potassium atoms trapped in a pure optical dipole trap. The scale on the right correspond to the optical density.
Source: By the author.

During the gray molasses stage the cloud is not being confined and is expanding during the stage, making it difficult to obtain a good mode-matching. We also have the manifold of the $F = 1$ state that we need to consider. To "clean" the states of our cloud we utilized a technique deployed in the work "All-optical cooling of 39K to Bose-Einstein condensation",[44] where we turn ON only one arm of the ODT during the gray molasses and apply a low field gradient after the GM, repelling the $m_F = 1$ that will escape along the arm of the ODT. The $m_F = 0$ were supposed to escape through the arms since it doesn't have a good confinement in this direction and the $m_F = -1$ will be trapped in the center of the ODT and captured when the second arm is turned ON. By performing this sequence only the $m_F = -1$ would reach the ODT stage. Due to a technical limitation, we couldn't remove all the power on the second arm during the first stage, having a leak of around 500 mW on the second arm. After done this process we measured that 2/3 of the atoms vanished from the trap, indicating the technique had worked (and it did, but the remaining atoms were mysteriously at the $m_F = 0$). At the end of the sequence we obtained around $1.6 \cdot 10^5$ atoms trapped in the center of the ODT.

5.2 Measuring the potassium Feshbach resonances

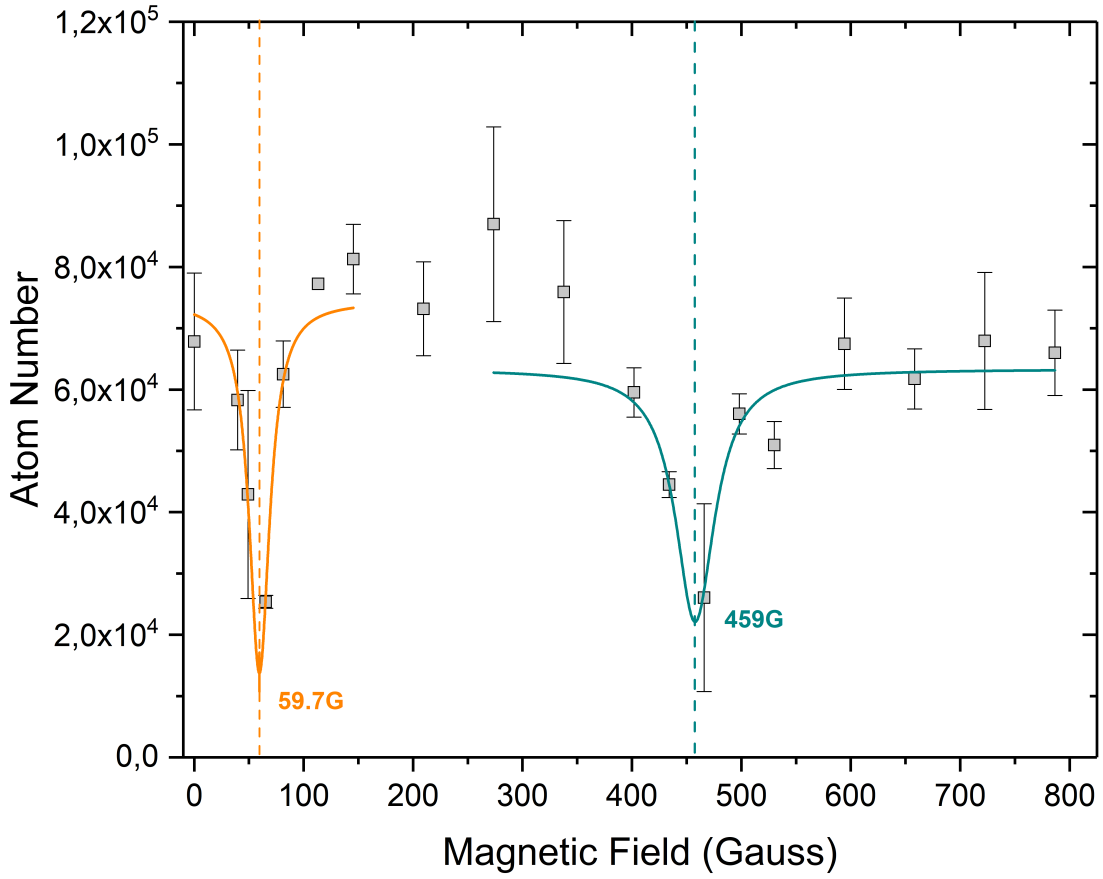

Figure 26 – The first Feshbach scan done by the group. We measured the remaining atoms in the ODT for each value of magnetic field applied. A Lorentzian was used to fit the atom number in the two regions we observed losses. The center of the losses were at 59.7 G and 459 G.

Source: By the author.

Once the potassium atoms are trapped in our optical dipole trap, we can begin tuning the Feshbach resonances. As mentioned earlier, we will use the same quadrupole coils to generate a uniform field in the region of the trap, switching the current of one of the coils using an H-Bridge. The method to locate the resonances is by loss spectroscopy, where we expect the trap to lose a considerable number of atoms when close to resonance due to the enhancement of inelastic losses. The atoms remain in the ODT for 100 ms before the Feshbach field is turned on abruptly. We choose to keep it on the atoms for 1 second before the trap is turned off for each value of the magnetic field, and the total

number of atoms remaining is observed. The first Feshbach scan can be seem in figure 26 where we fit the region of loss with a Lorentzian.

After some analysis of the magnetic field calibration we observed that we have two resonances near the first region (58.8 G and 65.6 G) and two resonances in the second region (471 G and 490 G). Finally we conclude that our cleaning method was not suitable and we had our sample in the state $F = 1, m_F = 0$ where we couldn't observe the resonances above 800 G due to the narrow width. At table 3 we show the points where we observed a severe loss in the atom number and the waist of each Lorentzian fitted. We tried to investigate the heating around the resonances, but we couldn't fit the cloud by a Gaussian properly at those points due to low atom number, resulting in a value that was not trustworthy at that moment.

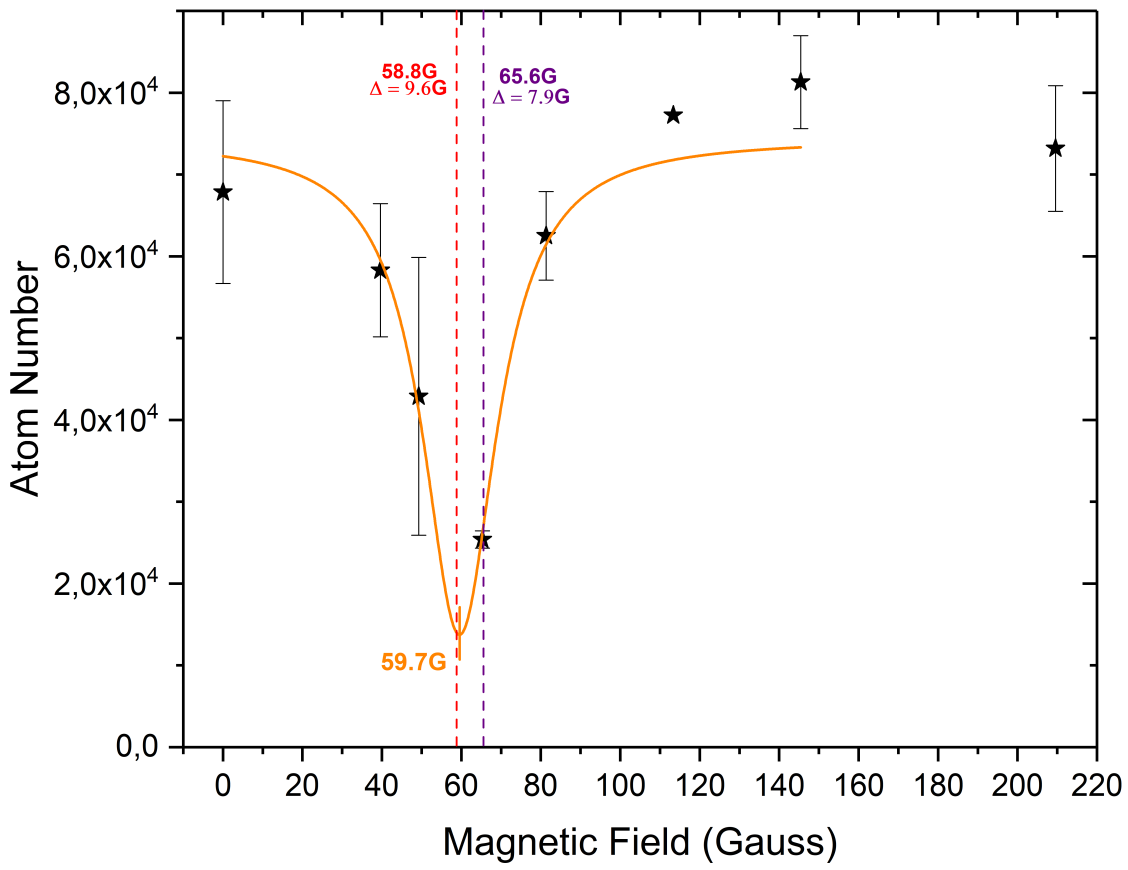

Figure 27 – A zoom at the first region of loss obtained at the first scan. The dashed lines correspond to the theoretical values of resonances in the $m_F = 0$. This graphic serve as a guide to the eye where there is a possibility the losses were due the two resonances.

Source: By the author.

We see that the first point we measured is between the first and second resonance, which has a similar width. As eye guidance we plotted in figure 27 two dashed lines where the first and second resonances are located with the corresponding width. We assume that the loss region is due to the first and second resonances, that we didn't have the resolution to differentiate them.

Table 3 – Feshbach resonances measured by loss spectroscopy for potassium 39 in $F = 1, m_F = 0$ state in this work. The B_0 is the center of the fitted Lorentzian and w is the waist of the Lorentzian

Resonance	B_0(G)	w(G)
1st	59.7	22.7
2nd	470.3	60

Source: By the author.

For the second resonance measured, we were able to redo the Feshbach scan and obtain a more stable measurement (see figure 28) wherein the center of the fitting we have around 60% fewer atoms than out of resonance. The agreement between the theoretical point and the experimental point was very good, probably due to this resonance having 72 G of width, wider than any other resonance in the $F = 1$ manifold. Another resonance is located at 490 G, but its width is so narrow that it may have been masked by the wider one, being necessary a higher resolution in the measurement to separate both. We pointed in figure 28 the points where the resonances are located with each width.

The reason why we remained only with the $m_F = 0$ did not reached a consensus between the team. One possible explanation is that the gradient used in the cleaning process were not high enough to trap the atoms, but since only the $m_F = \pm 1$ could feel it, they could be repelled by the trap like in a Stern-Gerlach pulse, if the center of the quadrupole is not exactly in the center of the ODT. Further investigation is needed before we reach a conclusion but it is clear that we have measured the mentioned resonances. In the next sub section we will provide one more evidence.

5.2.1 Comparing the lifetime of the samples

Since we couldn't measure the heating to validate more our measurement of the resonances, we have measured the lifetime of the sample for different scattering lengths. We have chosen three values: 466 G, 338 G and 0 G. The point 466 G corresponds to the second resonance observed dislocated 5 G to the left, 338 G corresponds to a point where we do not have a resonance near, and 0 G where the lifetime will be the ODT lifetime. A highly decrease was observed for the point near resonance (see figure 29), when compared to the other two curves, indicating the presence of a resonance near, increasing drastically

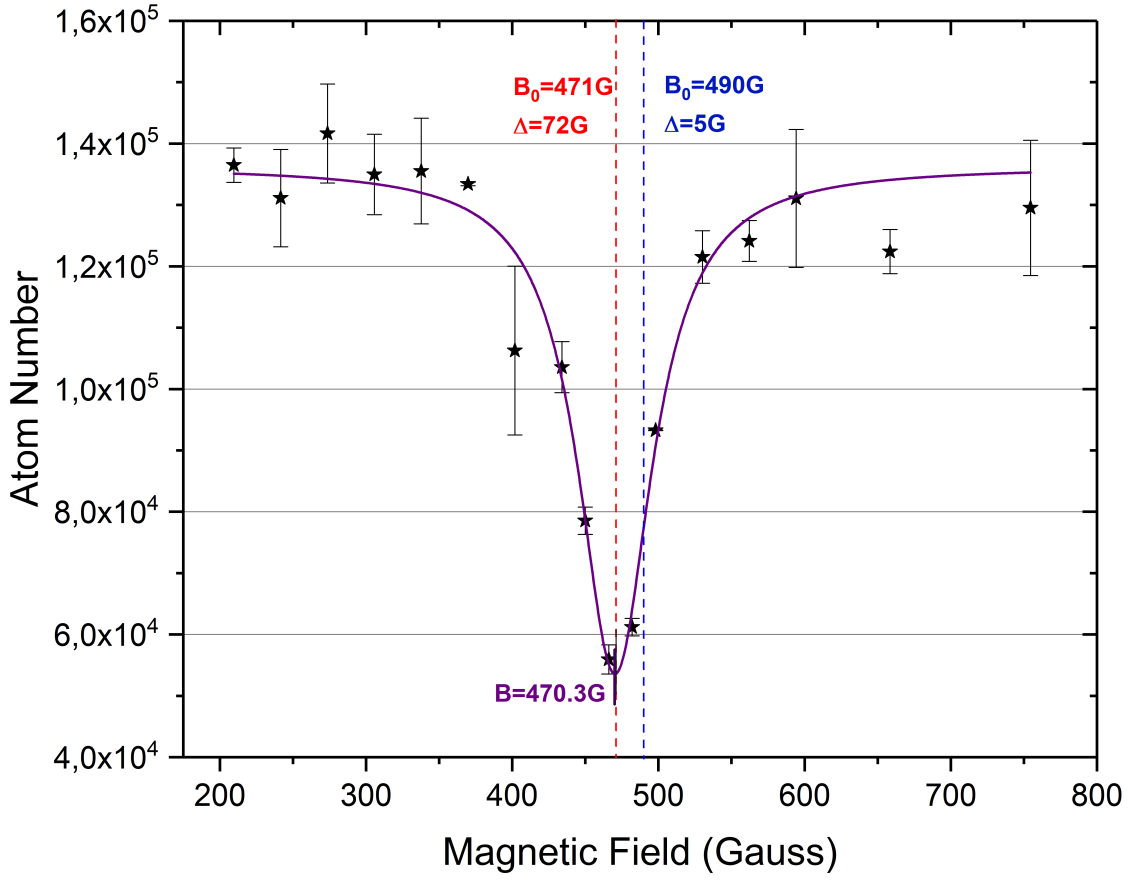

Figure 28 – Second scan of the second resonance observed. We fitted the experimental points with a purple Lorentzian and obtained a waist of 60 G with the center at 470.3 G. The dashed lines correspond to the theoretical value of the resonances, with each width.

Source: By the author.

the modulus of the scattering length, enhancing the inelastic losses. The points were fitted by two decaying exponentials, to take into account the two regimes where the first one being a dramatically fall due to the three-body losses before reaching a more stable regime. The lifetime measured near the resonance corresponding to the first decay of the sample were $\tau = 0.25$ s, with its points diverging from the other measurements that remained close.

We measured the lifetime of the sample with the field at 338 G to observe if the high field would be interfering in the lifetime measurement. The result was that the decaying was as if the field was turned off, with points close to the blue points in the graphic. These two curves were also fitted by two decaying exponentials and the lifetime corresponding to

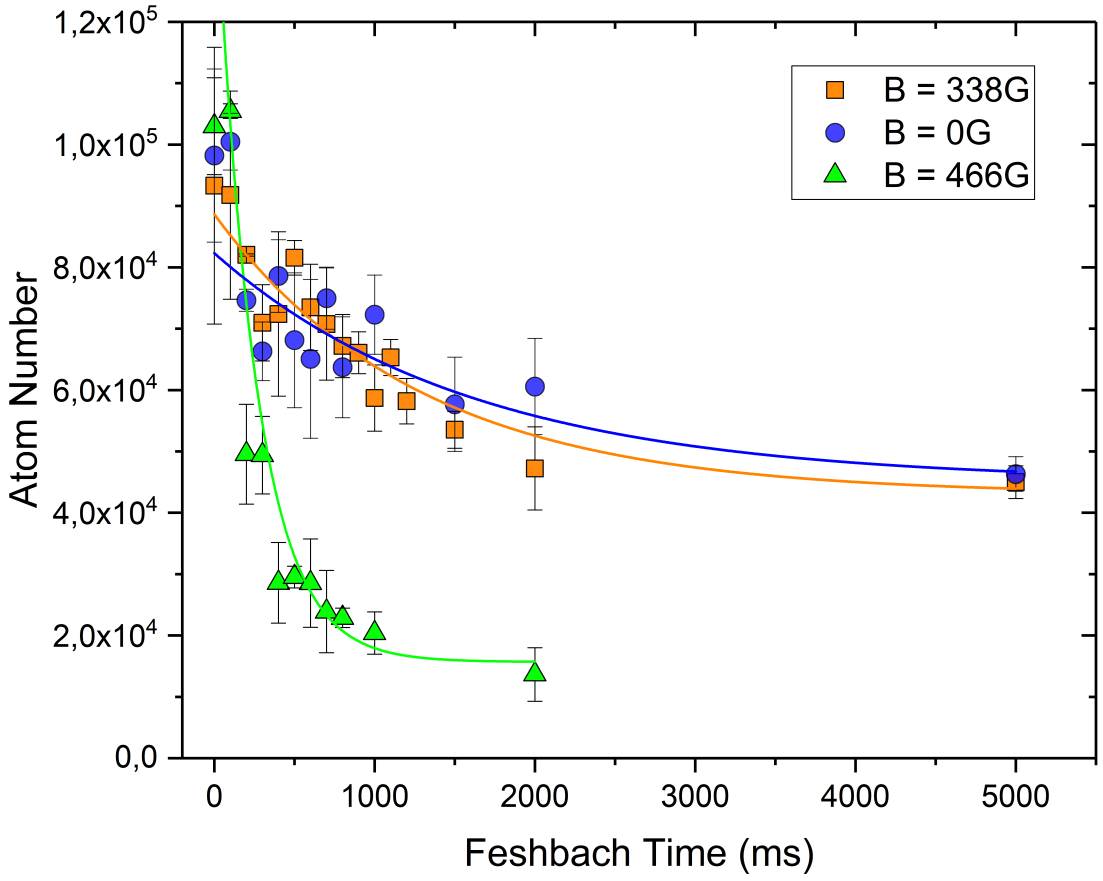

Figure 29 – Measurement of the lifetime of the atoms in the ODT for three different homogeneous magnetic field: B=0 G - field OFF - (blue circles), B=338 G (orange squares) and B=66 G (green triangles).
Source: By the author.

the first decay were very similar, measuring $\tau = 1.3$ s for the blue curve and $\tau = 1.6$ s for the orange curve. Our results are still very preliminary and need some investigation, but is indicating that we are indeed tuning the Feshbach resonances in our sample for the $|F = 1, m_F = 0\rangle$.

6 CONCLUSIONS AND PROSPECTS

In this work, we measured the Feshbach resonances for the potassium 39 in the state $|F = 1, m_F = 0\rangle$. We performed loss spectroscopy on the Optical-Dipole Trap and observed two regions of losses at around 59.7 G and 470 G, corresponding to the $m_F = 0$ state's resonances. The measurement was performed with the same pair of coils used in the quadrupole trap, switching it from anti-Helmholtz configuration to Helmholtz configuration in a very controllable way, using power IGBTs as fast switches. We ensure the tuning of the scattering length by performing a lifetime measurement, where the three-body and two-body (three-body mainly) are enhanced for a high scattering length.

We have decided to use potassium atoms as probes for the first measurements due to the accessible and wide Feshbach resonances, and the sodium lasers were not in good functionality. A few setbacks limited our measurements: The optical trap was built originally for the sodium that will sympathetic cool the potassium. We also faced signals of vacuum problems just after obtaining the measurements, interfering with the advance on steps as calibration of the field and the measurement of the resonances in the other states.

Even considering the fact that the inter-species resonances between sodium and potassium are wider than the ones measured in this work, we are still considering the implementation of a PID system to stabilize the magnetic field, providing us with higher resolution when performing loss spectroscopy. This first approach allowed us to obtain the first measurements and insights for the next stage of the general project. Having assured that the system is capable of tuning the Feshbach resonances we can continue with our aim to apply this technique in a double species Bose-Einstein condensate.

Now the sodium lasers are back from repair and we already have recovered the pressure in the Science Chamber. The sodium BEC was recovered and we observed the first signals of sympathetic cooling with both species in the magnetic trap. These studies will continue in the PhD, where we plan to obtain a double degenerate mixture where we will be capable to explore the different miscibility regimes and quenching effects in the sample.

REFERENCES

1 KETTERLE, W.; DURFEE, D. S.; STAMPER-KURN, D. **Making, probing and understanding Bose-Einstein condensates**. 1999, Available from: https://arxiv.org/pdf/cond–mat/9904034.pdf. Accessible at: 23 Jan. 2020.

2 LEE, K. L. *et al.* Phase separation and dynamics of two-component bose-einstein condensates. **Physical Review A**, APS, v. 94, n. 1, p. 013602, 2016.

3 VOGES, K. K. *et al.* Formation of ultracold weakly bound dimers of bosonic 23 Na 39 K. **Physical Review A**, APS, v. 101, n. 4, p. 042704, 2020.

4 DE, S. *et al.* Quenched binary Bose-Einstein condensates: spin-domain formation and coarsening. **Physical Review A**, APS, v. 89, n. 3, p. 033631, 2014.

5 CHIN, C.; GRIMM, R.; JULIENNE, P.; TIESINGA, E. Feshbach resonances in ultracold gases. **Reviews of Modern Physics**, APS, v. 82, n. 2, p. 1225, 2010.

6 INOUYE, S. *et al.* Observation of Feshbach resonances in a Bose–Einstein condensate. **Nature**, Nature Publishing Group, v. 392, n. 6672, p. 151–154, 1998.

7 CASTILHO, P. C. M. **New experimental system to study coupled vortices in a two-species Bose-Einstein condensate 23Na-41K with tunable interactions**. 2017. 216 p. Ph D. Thesis (Doctor in Science) — Instituto de Física de São Carlos, Universidade de São Paulo, São Carlos, 2017.

8 FARIAS, K. M. **Obtenção da degenerescência quântica em sódio aprisionado**. 2004. 102 p. Tese (Doutorado em Ciências) — Instituto de Física de São Carlos, Universidade de São Paulo, São Carlos, 2004.

9 PEÑAFIEL, E. E. P. **Production of a Bose-Einstein condensate of sodium atoms and investigation considering non-linear atom-photon interactions**. 2016. 175 p. Ph D. Thesis (Doctor in Science) — Instituto de Física de São Carlos, Universidade de São Paulo, São Carlos, 2016.

10 HENN, E. A. d. L. **Produçao experimental de excitaçoes topológicas em um condensado de Bose-Einstein**. 2015. 126 p. Tese (Doutorado em Ciências) — Instituto de Física de São Carlos, Universidade de São Paulo, São Carlos, 2015.

11 VIVANCO, F. A. J. **Investigations on momentum distributions and disorder in strongly out-of-equilibrium trapped Bose gases**. 2017. 120 p. Ph D. Thesis (Doctor in Science) — Instituto de Física de São Carlos, Universidade de São Paulo, São Carlos, 2017.

12 FRITSCH, A. R. **Thermodynamics of a Bose gas:** sound velocity from global variables and equivalence with other approaches. 2016. 106 p. Ph D. Thesis (Doctor in Science) – Instituto de Física de São Carlos, Universidade de São Paulo, São Carlos, 2016.

13 TAVARES, P. E. S. **Excitations in Bose-Einstein condensates:** collective modes, quantum turbulence and matter wave statistics. 2016. 134 p. Ph D. Thesis (Doctor in Science) – Instituto de Física de São Carlos, Universidade de São Paulo, 2016.

14 JOACHAIN, C. J. **Quantum collision theory**. Amsterdam: North–Holland Pub. Co., 1975.

15 REM, B. S. **The Road to the Unitary Bose Gas**. 2013. 217 f. Thése (Doctorat Physique Quantique) – Ecole Normale Supérieure de Paris, Paris, 2013.

16 CALLISTER, W. D. **Materials science and engineering:** an introduction. New York: Wiley, 2018.

17 SAKURAI, J. J. **Modern quantum mechanics**. Reading: Addison–Wesley Pub. Co., 1994.

18 WERNER, J. **Observation of Feshbach resonances in an ultracold gas of 52Cr**. 2006. 190 f. Ph D. Thesis (Doctor) — Physikalisches Institut, Universität Stuttgart, Stuttgart, 2006.

19 TIESINGA, E.; VERHAAR, B.; STOOF, H. Threshold and resonance phenomena in ultracold ground-state collisions. **Physical Review A**, APS, v. 47, n. 5, p. 4114, 1993.

20 COURTEILLE, P.; FREELAND, R.; HEINZEN, D.; ABEELEN, F. V.; VERHAAR, B. Observation of a Feshbach resonance in cold atom scattering. **Physical Review Letters**, APS, v. 81, n. 1, p. 69, 1998.

21 CHIN, C.; VULETIĆ, V.; KERMAN, A. J.; CHU, S. High resolution Feshbach spectroscopy of cesium. **Physical Review Letters**, APS, v. 85, n. 13, p. 2717, 2000.

22 MARTE, A. *et al.* Feshbach resonances in rubidium 87: Precision measurement and analysis. **Physical Review Letters**, APS, v. 89, n. 28, p. 283202, 2002.

23 LUDEWIG, A. *et al.* **Feshbach resonances in 40K**. 2012. 136p. Ph D. Thesis (Doctor) – Universiteit van Amsterdam, Amsterdam, 2012.

24 ROBERTS, J. L. *et al.* Controlled collapse of a Bose-Einstein condensate. **Physical Review Letters**, APS, v. 86, n. 19, p. 4211, 2001.

25 PAPP, S.; PINO, J.; WIEMAN, C. Tunable miscibility in a dual-species Bose-Einstein condensate. **Physical Review Letters**, APS, v. 101, n. 4, p. 040402, 2008.

26 WACKER, L. *et al.* Tunable dual-species Bose-Einstein condensates of K 39 and Rb 87. **Physical Review A**, APS, v. 92, n. 5, p. 053602, 2015.

27 SCHULZE, T. A. **Quantum degenerate mixtures of 23Na-39K and coherent transfer paths in NaK molecules**. 2018. Ph D. Thesis (Doctor) – Fakultät für Mathematik und Physik, Gottfried Wilhelm Leibniz Universität Hannover, Hannover, 2018.

28 CHIN, C.; KERMAN, A. J.; VULETIĆ, V.; CHU, S. Sensitive detection of cold cesium molecules formed on Feshbach resonances. **Physical Review Letters**, APS, v. 90, n. 3, p. 033201, 2003.

29 SCHMIDT, P. O. **Scattering properties of ultra-cold chromium atoms**. 2003. Ph D. Thesis (Doctor) — Physikalisches Institut, Universitat Stuttgart, Stuttgart, 2003.

30 LANDINI, M. **A tunable Bose-Einstein condensate for quantum interferometry**. 2012. Ph D. Thesis (Doctor) – University of Trento, Trento, 2012.

31 D'ERRICO, C. *et al.* Feshbach resonances in ultracold 39K. **New Journal of physics**, IOP Publishing, v. 9, n. 7, p. 223, 2007.

32 JOCHIM, S. *et al.* Bose-Einstein condensation of molecules. **Science**, American Association for the Advancement of Science, v. 302, n. 5653, p. 2101–2103, 2003.

33 SCHULZE, T. A. *et al.* Feshbach spectroscopy and dual-species Bose-Einstein condensation of 23Na-39K mixtures. **Physical Review A**, APS, v. 97, n. 2, p. 023623, 2018.

34 HALL, D.; MATTHEWS, M.; ENSHER, J.; WIEMAN, C.; CORNELL, E. A. Dynamics of component separation in a binary mixture of Bose-Einstein condensates. **Physical Review Letters**, APS, v. 81, n. 8, p. 1539, 1998.

35 CÓRDOVA, C. R. C. **Quantum liquid droplets in a mixture of Bose-Einstein condensates**. 2018. Ph D. Thesis (Doctor) – The Institute of Photonic Sciences, Universidad Politécnica de Cataluña, Cataluña, 2018.

36 MCCARRON, D.; CHO, H.; JENKIN, D.; KÖPPINGER, M.; CORNISH, S. Dual-species Bose-Einstein condensate of Rb 87 and Cs 133. **Physical Review A**, APS, v. 84, n. 1, p. 011603, 2011.

37 CASTILHO, P. C. M. A compact experimental machine for studying tunable bose-bose superfluid mixtures. **Laser Physics Letters**, v. 16, n. 3, p. 035501, 2019.

38 LAMPORESI, G.; DONADELLO, S.; SERAFINI, S.; FERRARI, G. Compact high-flux source of cold sodium atoms. **Review of Scientific Instruments**, American Institute of Physics, v. 84, n. 6, p. 063102, 2013.

39 SALOMON, G. *et al.* Gray-molasses cooling of 39K to a high phase-space density. **EPL (Europhysics Letters)**, IOP Publishing, v. 104, n. 6, p. 63002, 2014.

40 GRIMM, R.; WEIDEMÜLLER, M.; OVCHINNIKOV, Y. B. Optical dipole traps for neutral atoms. **Advances in Atomic, Molecular, and Optical Physics**, v. 42, p. 95–170, 2000.

41 WENZEL, M. **A dysprosium quantum gas in highly controllable optical traps**. 2015. Ph D. Thesis (Doctor) – Universitäet Stuttgart, Stuttgart, 2015.

42 CHENG, N. S. **Control of Feshbach resonant interactions in ultracold potassium-40 experiments**. 2012. (Master thesis), University of Toronto, Toronto, 2012.

43 KOHNEN, M. **Ultracold Fermi mixtures in an optical dipole trap**. 2008. Ph D. Thesis (Doctor) — Faculty of Physics and Astronomy, Universität of Heidelberg, Heidelberg, 2008.

44 SALOMON, G.; FOUCHÉ, L.; LEPOUTRE, S.; ASPECT, A.; BOURDEL, T. All-optical cooling of K 39 to Bose-Einstein condensation. **Physical Review A**, APS, v. 90, n. 3, p. 033405, 2014.